Cell Reports
Physical Science

CellPress
OPEN ACCESS

Review

Battery pack states, properties, and characterization techniques beyond cell level

Tom Rüther,[1,2,*] Wesley Hileman,[3] M. Scott Trimboli,[3] Gregory L. Plett,[3] Matthieu Dubarry,[4] Nikhil Kumar,[5] James Marco,[5] Franz Roehrer,[6] Andreas Jossen,[6] Jan Schöberl,[7] Markus Lienkamp,[7] Oliver Bohlen,[8] and Michael A. Danzer[1,2]

[1]Chair of Electrical Energy Systems, University of Bayreuth, Universitätsstraße 30, 95447 Bayreuth, Germany
[2]Bavarian Center for Battery Technology, University of Bayreuth, Universitätsstraße 30, 95447 Bayreuth, Germany
[3]Department of Electrical and Computer Engineering, University of Colorado Colorado Springs, 1420 Austin Bluffs Parkway, Colorado Springs, CO 80918, USA
[4]Hawaii Natural Energy Institute, University of Hawaii at Manoa, 1680 East-West Road, Honolulu, HI 96822, USA
[5]Warwick Manufacturing Group, University of Warwick, Gibbet Hill Road, CV47AL Coventry, UK
[6]Chair of Electrical Energy Storage Technology, Technical University of Munich, Karlstraße 45-47, 8033 Munich, Germany
[7]Institute of Automotive Technology, Technical University of Munich, Boltzmannstraße 15, 85748 Garching, Germany
[8]Institute for Sustainable Energy Systems ISES, Munich University of Applied Sciences, Lothstraße 64, 80335 Munich, Germany
*Correspondence: tom.ruether@uni-bayreuth.de
https://doi.org/10.1016/j.xcrp.2025.102919

SUMMARY

Battery packs, defined as interconnections of individual cells, are central to modern energy systems, yet their electrical and electrochemical behavior remains insufficiently understood. This review consolidates foundational principles, outlines challenges, and addresses fragmented knowledge that hinders further development at the pack level. A key challenge is the lack of harmonized and uniquely defined states, such as the state of charge and the state of health. To address this, we propose revised definitions and introduce state descriptors for more consistent and comparable pack-level analysis. We critically evaluate existing characterization methods, originally developed for single cells, and highlight their potential and limitations at the pack level. Many of these methods require further adaptation, and only their combination with harmonized state descriptors enables reliable and meaningful results. This work goes beyond identifying challenges by closing gaps in state descriptions, providing a foundation for future research, fostering reliable diagnostics, and supporting innovation in energy storage technologies.

INTRODUCTION

Rechargeable batteries with high power and energy density are the cornerstone of portable and mobile applications. They are enablers for developing and employing power tools, robots, and electromobility. In stationary energy systems, battery-energy storage systems play a central role in providing flexibility and stability. Economic studies indicate an immense growth potential for battery systems across all the aforementioned fields.[1,2]

Presently, and for the foreseeable future, lithium-ion batteries (LIBs) are the predominant storage technology for all applications.[1] Recently, sodium-ion batteries entered the market as an economical drop-in technology with the same system design as LIBs.[3] Compared to other technologies, such as lead-acid batteries, LIBs, in most cases, require thermal management, battery monitoring, and management systems. Except for wearable and small portable devices, multiple electrochemical cells are integrated into battery modules or packs to ensure that they meet the application-specific performance and energy requirements.[4,5]

The electrical and electrochemical properties and the behavior of these multi-component systems play a pivotal role in determining the performance, safety, and longevity of the battery pack. The connection of cells to make a module or pack poses major challenges to the understanding, development, and operation of the energy storage system that are not present in single cells. Hence, the whole is more than the sum of its parts. In other words, the complex system exhibits properties or behaviors that its parts do not possess individually and that emerge as a result of their interactions. This emergence is the core focus of this work. Despite its critical importance, the foundational principles that govern the electrical and electrochemical properties and the behavior of battery systems are fragmented, contradictory, and incomplete across the existing literature.

A major challenge in this domain pertains to the absence of harmonized definitions for fundamental battery states, including the state of charge (SoC), the state of health (SoH), and the state of energy (SoE). These metrics and operational variables, which are essential for assessing battery performance and for operating battery systems, are often defined inconsistently at the pack level and vary significantly depending on the application or experimental context. Furthermore, pack states are not uniquely defined, which can lead to significantly different battery pack behavior despite the same state indicators. This variability

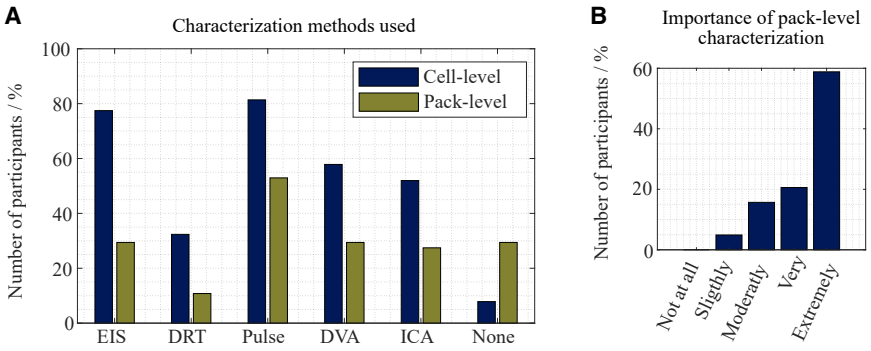

Figure 1. Survey results on pack-level characterization

Results of the battery pack characterization survey, which was completed by 102 participants and includes results from a total of 18 countries. Percentage of survey respondents who have used electrochemical impedance spectroscopy (EIS), distribution of time constants (DRT), pulse test, differential voltage analysis (DVA), incremental capacity analysis (ICA), or none of these characterization methods at the cell or pack level.

(A) Number of respondents who rate the importance of pack-level characterization as not at all important, very important, moderately important, extremely important, or extremely important.

(B) Further data from the survey can be found in Note S1.

not only complicates the interpretation of individual results but also creates barriers to comparing studies, ultimately hindering progress in understanding and optimizing battery systems.

Despite the noteworthy advancements in research at the cell level in recent years, the electrical and electrochemical characterization of battery packs has received comparatively less attention. Characterization methods, originally developed for single cells, offer a great potential for battery packs in terms of state description and diagnostics, as well as analysis of inhomogeneities and aging. The integration of cells in packs introduces a multitude of complexities, including interactions between cells, current distribution, manufacturing variations, and additional system components, such as cell connectors. As a result, the interpretation of pack-level characterization represents the second major challenge. The superposition of heterogeneous cell responses and parasitic effects obscures the underlying phenomena. Only the combination of a detailed understanding of multi-component interactions, a clear and consistent definition of pack-level states, and characterization methods tailored to the pack level enables reliable interpretation of results. Despite the paramount importance of this research area, no scientifically accepted approaches for the electrical and electrochemical characterization of the properties and behavior of battery modules have been established.

This gap is highlighted by a survey conducted as part of this study, which reveals a predominant research focus on cell-level characterization, while comparatively less attention is given to module-level approaches, as illustrated in Figure 1A. This finding is particularly concerning given the widespread use of multi-cell battery systems and the fact that the majority of survey participants consider pack-level characterization to be extremely important, as shown in Figure 1B. It is imperative to acknowledge the critical need for a systematic evaluation of methodologies and characterization techniques, as well as a common understanding of battery states at the module and pack levels.

The objective of this review is to address the aforementioned questions, challenges, and gaps by means of the following.

(1) The consolidation of the fundamental principles of battery pack electrical and electrochemical properties and behavior, which are currently scattered across the existing literature.
(2) A critical analysis of the definitions of key battery states at the pack level and their implications for research, development, and application, as well as an attempt to derive harmonized descriptive and prescriptive definitions.
(3) A comprehensive review and synthesis of the diverse approaches to pack-level characterization, with particular attention to their practical applicability and limitations.

This review provides a comprehensive overview of the subject matter, with the objective of serving as a leverage point for researchers, developers, and practitioners in the field of battery pack characterization. It aims to promote clarity and consistency in the field, enable a more profound comprehension of the electrical and electrochemical properties of battery packs, and facilitate the development of enhanced solutions for energy-storage systems and their operation. To this end, this work not only summarizes the existing literature but also introduces new definitions to provide a basic reference for an emerging field of research poised for significant growth.

The statements and conclusions presented in this work pertain to multi-cell battery systems, irrespective of their specific cell technology. Most of the discussed principles and phenomena apply across various cell chemistries. However, for emerging chemistries, such as silicon-based electrodes or sodium-ion batteries, certain specific characteristics or principles may differ from the effects described in this paper.

FUNDAMENTALS OF BATTERY PACKS

Cell-to-cell variations

Variations in capacity and impedance among new lithium-ion cells arise due to manufacturing tolerances,[6–9] storage conditions, and shipping processes.[10] These initial discrepancies increase over time and are exacerbated by non-uniform current distribution[6,8,11] and temperature[6,12] variations, leading to accelerated[10,13–15] or inhomogeneous[10,15–17] aging. Understanding and responding to these cell-to-cell variations (CtCvs) is therefore essential to ensure the reliability and longevity of battery packs. The causes of CtCv are diverse and span multiple levels, from materials to cells, modules, and packs. Beck et al.[18] provide a comprehensive literature review that differentiates between intra-cell variations, arising from differences in materials

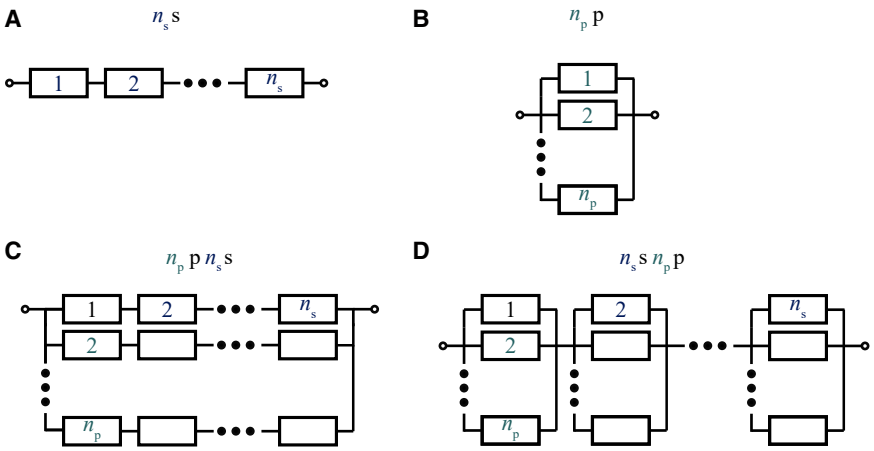

Figure 2. Topologies of battery packs
Serial (A), parallel (B), parallel-serial (C), and serial-parallel (D) connection topologies.

and electrodes, and inter-cell variations, which account for differences between cells, affecting management and operation from the cell to the pack level. Most studies in the literature have focused on parametric analyses, examining key factors such as capacity, resistance, differential voltage analysis (DVA) features, and a broad spectrum of impedance characteristics. A detailed synthesis of these findings is provided in Table S1.

Dubarry et al.[19] attributed CtCv to differences in active material content, polarization resistance, and kinetic limitations. An investigation[20] into the performance of new and aged EV cells revealed a systematic shift in the distribution of key parameters. While these parameters initially follow a normal distribution, continued operation leads to a transition toward a left-skewed Weibull distribution. This shift is accompanied by an increasing number of statistical outliers, indicating that aging and usage conditions amplify variations between individual cells. Furthermore, the cycling rate of a battery significantly influences the evolution of CtCv. Higher charge and discharge rates amplify kinetic limitations, leading to greater disparities in impedance, resistance, and capacity retention.[21] A statistical evaluation of 1,100 lithium-ion cells found no correlation between capacity and impedance. Additionally, different batches exhibited distinct statistical characteristics, suggesting potential manufacturing variations.[10] An investigation using the distribution of relaxation times (DRT) method explored CtCvs in LIBs and their impact on electrochemical processes. The study identified distinct correlations between electrode processes and revealed deviations from commonly assumed statistical distributions, suggesting more complex underlying variations.[22]

Thus, CtCvs exhibit distinct statistical properties that evolve over time and are inherently dependent on individual cell characteristics. These variations become particularly relevant when analyzing different interconnect topologies.

Topologies and components

To meet the voltage and capacity requirements of modern applications, cells are assembled into battery packs using various interconnect topologies. These topologies can be broadly categorized into series connections, which increase voltage, and parallel connections, which increase charge and current capacity. In addition, approaches combining both strategies are possible. A standardized nomenclature has been established to describe these different interconnect topologies, as shown in Figure 2.

The impact of CtCv on different interconnection topologies has been extensively studied. Dubarry et al.[23] demonstrated that CtCvs affect voltage response and capacity, with parallel configurations being significantly more resilient due to internal balancing. Luan et al.[24] further explored various module architectures and identified parallel-serial topologies as the most effective in optimizing capacity retention and discharge performance. Similarly, Porpora et al.[25] found that capacity imbalances exert the most pronounced influence on overall pack efficiency and degradation. Expanding on these findings, Kim and Choi[26] systematically evaluated the effects of CtCv across multiple performance metrics. According to Lingzhao et al.,[27] performance in serial connections is dominated by capacity discrepancies, self-discharge, and SoC mismatches, while in parallel connections, capacity and resistance variations impact current distribution and thermal stability.

In addition to CtCv and topology, joining technology and pack architecture are critical factors influencing battery pack performance.

Joining technologies

For efficient and reliable battery connections, two primary architectures are commonly employed: busbar-based configurations and direct wiring without busbars, as schematically illustrated in Figure 3. Tab-to-busbar joining, encompassing classic, laminated, and flexible printed circuit busbars, offers low resistance and high current-carrying capacity, making it the preferred choice for demanding applications. In contrast, tab-to-tab solutions, such as cable connections and nickel strips, are easier to assemble but have higher resistance and greater thermal stress, limiting their applicability.

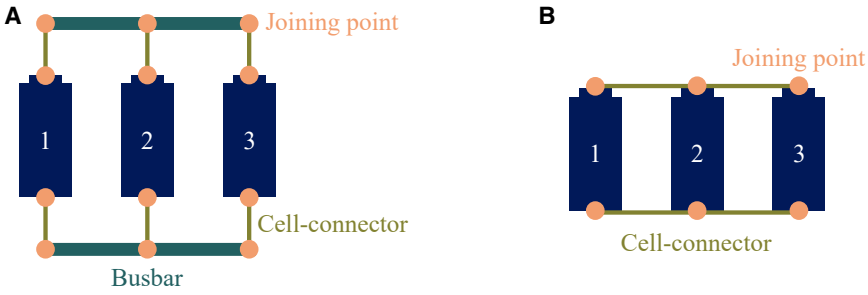

Figure 3. Common architectures for battery packs

Schematic representation of a tab-to-busbar joining (A) and a tab-to-tab joining (B) for battery packs for a parallel connection of 3 cells.

Beyond this, there are alternative interconnect approaches that optimize specific aspects of performance and manufacturability. Examples include crimp and plug-in connections that facilitate modularity and serviceability and conductive polymer foams that enhance mechanical flexibility while maintaining electrical conductivity.

The choice of interconnection architecture influences the number and placement of joining points. Studies on optimal terminal positioning are available in the literature,[26,28,29] while the focus of this section will be on joining technologies. These often require the joining of dissimilar materials, such as copper and aluminum. A wide range of joining technologies is available, each with distinct properties in terms of mechanical stability, thermal effects, electrical impedance, automation feasibility, and repairability. The selection of an appropriate technique depends on the specific design requirements of the battery pack, as different methods offer trade-offs in terms of performance and manufacturability. A comprehensive comparison of currently used joining technologies is provided in Table 1.

Among these methods, laser welding is most widely used due to its numerous advantages, including non-contact operation, narrow heat-affected zones, localized heat input, and high welding speeds.[30] This process uses a high-energy laser beam to create a localized melt pool, forming a low-resistance joint.[30] It allows precise control but requires optimized parameters to minimize heat-affected zones.[31] Resistance spot welding joins materials by applying electric current and mechanical pressure to create a fused joint. It is widely used because of its scalability; however, electrode wear increases contact resistance over time, affecting long-term performance. Nevertheless, it remains a viable option for smaller applications due to its lower initial investment and maintenance costs.[30,32] Ultrasonic welding uses high-frequency vibrations to create a solid bond, eliminating the need for melting and reducing thermal effects. It provides stable electrical resistance over extended cycles and improved thermal stability.[30] However, bond degradation can occur at high current densities, and its application is mainly limited to thin materials.[33]

Several studies have systematically compared these three welding techniques. Brand et al.[34] used the four-point probe method to assess electrical contact resistance and found that laser welding produced the strongest joints with the lowest resistance. Similarly, Larsson et al.[35] investigated cost, automation potential, and weld quality in the context of battery assembly. Their analysis highlighted laser welding as the optimal choice for high-volume production due to its high degree of automation, while resistance spot welding remained the preferred choice for smaller-scale applications due to its lower equipment costs. Ultrasonic welding, on the other hand, was noted for its versatility in joining a wide range of materials.

In addition to conventional techniques, several alternative approaches have been explored. While these methods are still uncommon in large-scale battery manufacturing, they offer distinct advantages in terms of repairability. Adhesive bonding uses conductive epoxies to make electrical connections without thermal input. However, this approach typically has a higher initial contact resistance, and long-term studies indicate that conductivity degrades under elevated temperatures and cyclic loading.[30,36] Mechanical fasteners, including screws and clamps, facilitate easy disassembly and repair but can introduce higher contact resistance[37,38] and susceptibility to vibration-induced instability.[39] Optimizing contact pressure and selecting appropriate coatings are critical to minimizing resistance and ensuring long-term reliability.[30,40]

For a more detailed discussion of this topic, as well as additional joining methods, the reader is referred to the literature review by Zwicker et al.[30]

The choice of joining technology directly affects the impedance of the pack, thereby influencing electrochemical characterization and potentially limiting overall pack performance in the event of degradation or failure. Most critically, impedance determines the current distribution between cells connected in parallel, with significant implications for safety, performance, and lifetime.

Batteries connected in parallel

Connecting cells in parallel to create a battery pack increases capacity while allowing the use of smaller standardized cells, greater flexibility in pack design, improved cooling and heating, and increased reliability compared to using single, larger cells.[11,41]

The parallel connection forces equal voltages:

$$U_{\text{parallel}} = U_i + U_{\text{con},i} = U_j + U_{\text{con},j} \quad \forall \quad i,j \in [1, n_p], i \neq j \qquad \text{(Equation 1)}$$

with U_{parallel} being the voltage of the parallel connection, n_p the number of parallel connected cells, U_i as the voltage of the respective cell i, and $U_{\text{con},i}$ accounting for the voltage drop across all contact resistances within parallel path i, including the relevant joining points and the corresponding part of the busbar. The effect of inhomogeneous resistances on the current distribution has been investigated by Jocher et al.[42] and Roehrer et al.[43] However, assuming negligible contact resistances or

Table 1. Comparison of joining technologies for cell-to-busbar battery connections

Method	Mechanical stability	Thermal impact	Automation feasibility	Repairability	Admittance
Laser welding	+	o	+	-	++
Resistance spot welding	o+	o	+	-	+
Ultrasonic welding	o	+	o	o	+
Adhesive bonding	o	++	o	+	-
Mechanical fastening	o	++	o	++	-

Joining technologies are rated as very good (++), good (+), medium to good (o+), medium (o), medium to poor (o–), poor (-), and very poor (– –) based on mechanical stability, thermal impact, automation feasibility, and repairability.

their equal inclusion in the voltage responses of the individual cells, the parallel connection enforces equal cell voltages:

$$U_{\text{parallel}} = U_i = U_j \quad \forall \quad i,j \in [1, n_p], i \neq j \qquad \text{(Equation 2)}$$

Consequently, voltage cannot be distinguished between individual cells, leading to parallel connections often being referred to as logical cells, cell blocks, or macro cells. The capacity of a logical cell C_{parallel} is determined through the sum of the individual capacities C_i,

$$C_{\text{parallel}} = \sum_{i=1}^{n_p} C_i, \qquad \text{(Equation 3)}$$

and the resistance of a logical cell R_{parallel} is determined using

$$R_{\text{parallel}} = \frac{1}{\sum_{i=1}^{n_p} R_i^{-1}}, \qquad \text{(Equation 4)}$$

where R_i is the resistance of the individual cells and contact resistances are neglected. As a result, the resistance of a logic cell is always lower than that of a single cell.

The power of a logical cell is typically described through its pulse-power capability (PPC), which is the maximum charge or discharge power a pack can handle via a current pulse I_{parallel} without exceeding the upper voltage limit U_{max} or dropping below the lower voltage limit U_{min}.[44] It is determined using the DC resistance R_{DC}, which is calculated using

$$R_{\text{DC}} = \frac{\Delta U_{\text{DC}}}{I_{\text{pulse}}} \qquad \text{(Equation 5)}$$

using the change in voltage ΔU_{DC} of the pack to a current pulse I_{pulse} of a typical duration of t_{pulse} = 10 s. The value of this resistance depends on whether the pack is being charged or discharged, which is why it is denoted as $R_{\text{DC,ch}}$ and $R_{\text{DC,dc}}$, respectively. This resistance is a function of several factors, including the SoC, SoH, temperature, and various other cell- and pack-level parameters. Assuming a purely ohmic voltage response in the parallel circuit, it is possible to determine the maximum permissible current without exceeding voltage limits. Consequently, the PPC of a parallel connection PPC_{parallel} is given by

$$PPC_{\text{parallel}} = \begin{cases} I_{\text{max,ch}} \cdot U_{\text{max}} = \dfrac{(U_{\text{max}} - U_{\text{OCV}})}{R_{\text{DC,ch}}} \cdot U_{\text{max}}, \text{for charge} \\ I_{\text{max,dc}} \cdot U_{\text{min}} = \dfrac{(U_{\text{OCV}} - U_{\text{min}})}{R_{\text{DC,dc}}} \cdot U_{\text{min}}, \text{for discharge} \end{cases}, \qquad \text{(Equation 6)}$$

with $I_{\text{max,ch}}$ and $I_{\text{max,dc}}$ being the maximum applicable current without violating the voltage limits of the respective charge and discharge cases. In practice, this current may exceed the data sheet limit, which must then be used to calculate the PPC.

The total energy of a logical cell E_{parallel} is determined by

$$\begin{aligned} E_{\text{parallel}} &= \int_{t(SoC=0)}^{t(SoC=1)} I_{\text{parallel}} \cdot U_{\text{parallel}} \, dt \\ &= C_{\text{parallel}} \int_{SoC=0}^{SoC=1} U_{\text{parallel}}(SoC) \, dSoC, \end{aligned} \qquad \text{(Equation 7)}$$

with I_{parallel} being the current of the logical cell. This current is the sum of the individual cell currents I_i:

$$I_{\text{parallel}} = \sum_{i=1}^{n_p} I_i. \qquad \text{(Equation 8)}$$

Given identical cells (open-circuit voltage [OCV] and impedance), identical operating conditions (temperature and SoC), and identical contacts, each cell carries a similar current, ensuring symmetric operation.

In the case of non-identical cells or inhomogeneous conditions, the current distribution among cells becomes unequal, depending on the local slope of the OCV curves and the cell impedances.[11,45] An analytical, simplified description of the current distribution, based on an equivalent cell circuit with a linear OCV characteristic and a constant cell resistance R, is provided by Fill et al.[46] For two parallel cells with the initial condition of identical SoCs, they derived the following current distribution:

$$\frac{I_1}{I_{\text{parallel}}} = \frac{C_1}{C_1+C_2}\left[\left(\frac{R_2}{R_1+R_2} \cdot \frac{C_1+C_2}{C_1} - 1\right) \exp\left(-\frac{t}{\tau}\right) + 1\right], \qquad \text{(Equation 9)}$$

with time t. The time constant τ is determined through

$$\tau = \frac{(R_1+R_2) \cdot C_1 \cdot C_2}{m_{\text{OCV}} \cdot (C_1+C_2)}, \qquad \text{(Equation 10)}$$

where $m_{\text{OCV}} = \frac{dOCV}{dSoC}$ is the slope of the OCV.

For a constant-current step, the initial-current distribution is defined by the cell resistances only by

$$\frac{I_1(t=0)}{I_{\text{parallel}}} = \frac{R_2}{R_1+R_2}. \qquad \text{(Equation 11)}$$

After a transient process, the current distribution reaches an equilibrium,

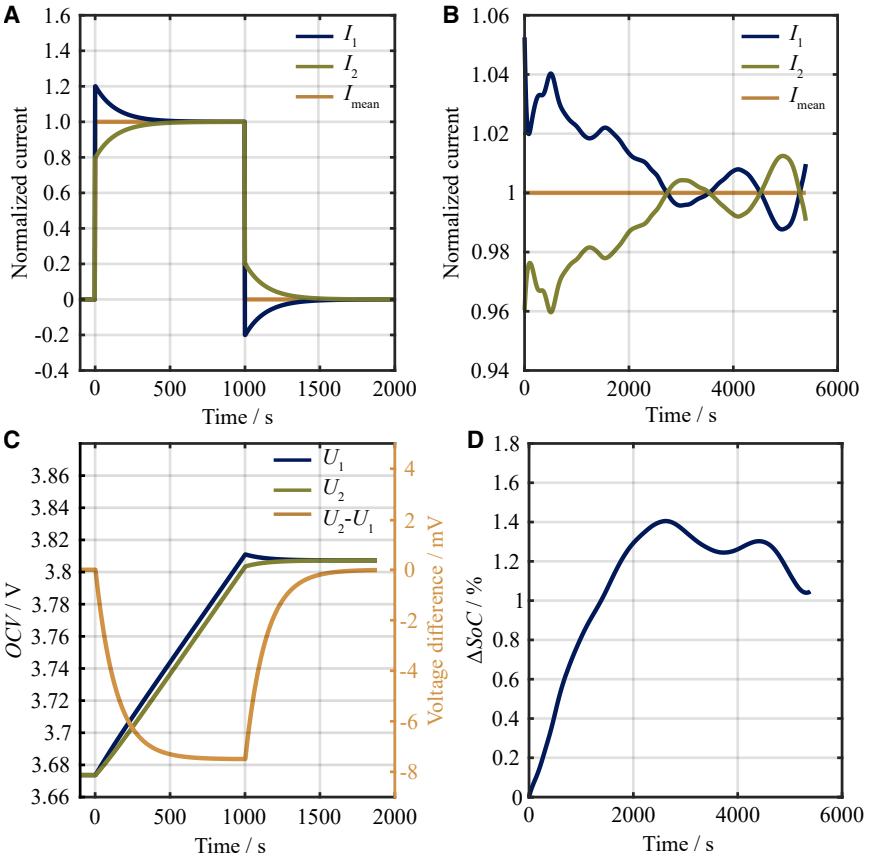

Figure 4. Current distribution in parallel-connected battery packs

(A and C) Current distribution (A) and open-circuit voltage differences (C) simulated using a simplified model under a scenario where individual cells have varying internal resistances and equal capacities, for a 100 s charging pulse with two parallel-connected cells, based on data from Brand et al.[11]

(B and D) Laboratory investigation of current distribution (B) and SoC differences (D) under a similar scenario for NCA cells, based on data from Jocher et al.[42]

$$\frac{I_1(t\to\infty)}{I_{parallel}} = \frac{C_1}{C_1+C_2} \qquad \text{(Equation 12)}$$

which is defined by the cell capacities. In this equilibrium, the differences in OCV ΔU_{OCV} can be described using

$$\frac{\Delta U_{OCV}(t\to\infty)}{I_{parallel}} = \frac{R_1C_1 - R_2C_2}{C_1+C_2}. \qquad \text{(Equation 13)}$$

Interrupting the current flow reveals a transient behavior as the cells return to balance, characterized by an exponential current decay. Figure 4A illustrates the current distribution based on the above model with a scenario of different cell resistances.

Further enhancements to these models incorporate nonlinear OCV behavior, as detailed by Fill et al.,[47] and employ complex impedance parameters instead of simplistic cell-resistance representations.[48] These improvements allow for a more accurate representation of the dynamic interactions within parallel-connected cells.

Jocher et al.[42] studied the current distribution in parallel-connected cells with different chemistries and demonstrated that nonlinear differences in the OCV characteristics can lead to significant variations in the current distribution. As shown for an NCA cell in Figure 4B, such variations can lead to inhomogeneous current distribution and even current reversals. These effects are strongly dependent on the cell chemistry, with LFP cells exhibiting significantly larger deviations than NCA cells. For example, under a 10 K temperature gradient, a 0.5 C constant-current charge resulted in SoC differences of up to 10% near the end of charge for LFP cells, due to their characteristically low voltage slope. In contrast, NCA cells showed only small SoC deviations of around 2% under identical conditions. More generally, the OCV characteristics of the logical cell become increasingly blurred due to inhomogeneous SoC distributions between the cells connected in parallel.

Furthermore, the aging behavior of parallel-connected cells differs from that of single cells, with many studies reporting accelerated aging under temperature gradients,[15,49,50] whereas Schindler et al. demonstrated improved lifetimes under homogeneous temperature conditions.[51]

Batteries connected in series

Connecting individual cells or logical cells in series in a battery pack increases voltage, reduces power losses in cables, improves efficiency, and simplifies power-electronics integration. Most importantly, it allows for high-voltage charging, significantly reducing charging times.

The voltage of a serial connection U_{serial} is determined through the voltage of the individual cells U_i and the voltage of the contact resistances U_{con}, including the relevant joining points and the corresponding portion of the busbar of all n_s connected cells:

$$U_{serial} = \sum_i^{n_s} U_i + \sum_i^{n_s} U_{con,i}. \qquad \text{(Equation 14)}$$

If the contact resistances are neglected or equally included in the voltage responses of the individual cells, the series connection can be described by

$$U_{serial} = \sum_i^{n_s} U_i. \qquad \text{(Equation 15)}$$

Unlike a single logical cell, battery packs with series-connected cells require careful monitoring of individual cell limits.

The total resistance R_{serial} of serially connected cells is determined from the sum of the individual resistances R_i of the cells using

$$R_{serial} = \sum_{i}^{n_s} R_i. \quad \text{(Equation 16)}$$

The capacity of a serial connection is ideally equal to that of the individual cells C_i. Due to CtCv, the discharge $C_{serial,\ discharge}$ and charge capacity $C_{serial,\ charge}$ are limited by the lowest capacity using[52–55]

$$C_{serial,discharge} = \min\{C_{1,discharge}, C_{2,discharge}, \ldots, C_{n_s,discharge}\} \text{ and} \quad \text{(Equation 17)}$$

$$C_{serial,charge} = \min\{C_{1,charge}, C_{2,charge}, \ldots, C_{n_s,charge}\}. \quad \text{(Equation 18)}$$

Since physical cells have imperfect Coulombic efficiency, the capacity of the battery pack is given through the discharge capacity $C_{serial} = C_{serial,\ discharge}$.

The minimum dischargeable (chargeable) capacity is therefore the amount of charge that can be removed from (put into) the pack before one of the cells is fully discharged (charged). However, the usable capacity of the pack can reach $C_{serial} = 0$ if one cell is in its fully charged state while another cell is in its fully discharged state, where the pack can be neither charged nor discharged without violating a voltage limit.[56] In contrast to cell capacity, which typically decreases monotonically with the age of a cell, it is possible for C_{serial} to increase when cells move from imbalanced to equalized or balanced states. This phenomenon is hereafter referred to as temporary or virtual capacity loss.

Cell imbalance arises from intrinsic heterogeneities between cells. Long-term SoC divergence between cells is driven by differences in Coulombic efficiency and self-discharge rates, which accumulate over cycling. In contrast, short-term imbalances—such as those due to varying capacities—are transient and self-correcting. While cell resistance does not directly affect the SoC, it limits the pack's power and energy availability by triggering voltage constraints earlier. A more detailed description of the causes of imbalances is provided by Plett.[4]

Cell equalization can be achieved through passive or active balancing strategies. Passive balancing dissipates excess charge as heat, whereas active balancing redistributes excess charge from cells with a high SoC to those with a lower SoC, improving energy utilization efficiency.[57–59] Active balancing methods employ relays, DC-DC converters, and/or current transducers in different configurations to achieve charge redistribution.[57] Both methods utilize either voltage-based or capacity-based algorithms for operation. In most cases, passive balancing exhibits energy losses an order of magnitude higher than those of active balancing approaches. The efficiency differences among balancing strategies across different battery topologies are discussed in detail by Baronti et al.[60] A comprehensive overview of existing approaches is presented in Figure 5, while a comparative summary of the available balancing methods and their advantages and disadvantages is presented in Table S2. Additional insights into these methodologies can be found in literature reviews.[52,57,61–63]

The PPC of a serial connection is constrained by the cell having the lowest power capability, which sets the upper limit on the pack's allowable current:

$$I_{PPC,max} = \min_{[i \in 1,\ldots,n_s]} \{|I_{PPC,i}|\}. \quad \text{(Equation 19)}$$

As shown in Figures 6A and 6B, the remaining cells are unable to utilize their potential power output fully. Consequently, the PPC of a serial connection PPC_{serial} is determined using

$$PPC_{serial} = \begin{cases} I_{PPC,max} \cdot \left(n_s \cdot U_{max} - \sum_i^{n_s} U_{OCV,i} - I_{PPC,max} \sum_i^{n_s} R_{DC,ch,i} \right), I_{PPC,max} > 0 \text{ (charge)} \\ I_{PPC,max} \cdot \left(\sum_i^{n_s} U_{OCV,i} - n_s \cdot U_{min} + I_{PPC,max} \sum_i^{n_s} R_{DC,dc,i} \right), I_{PPC,max} < 0 \text{ (discharge)} \end{cases}. \quad \text{(Equation 20)}$$

The total energy of the serial connection E_{serial} is determined using

$$E_{serial} = \int_{t(SoC_{pack}=0)}^{t(SoC_{pack}=1)} IU_{serial}\ dt = C_{serial} \sum_i^{n_s} \int_{SoC_{pack}=0}^{SoC_{pack}=1} U_i(SoC_{pack})\ dSoC_{pack}, \quad \text{(Equation 21)}$$

which is a function of the individual cell voltages U_i. The integral is evaluated over the full SoC range from $t(SoC_{pack} = 0)$ to $t(SoC_{pack} = 1)$. However, as the SoC of a battery pack is not yet well defined, a direct computation of the corresponding integral remains challenging. For a detailed discussion of the battery pack SoC definitions, we refer the reader to the next section and to Plett.[4] Since each cell exhibits a distinct voltage-capacity relationship, the corresponding integral varies across cells. As a result, the total extractable energy from the pack is ultimately limited by the cell with the lowest available energy. Figure 6C shows a schematic representation of this effect.

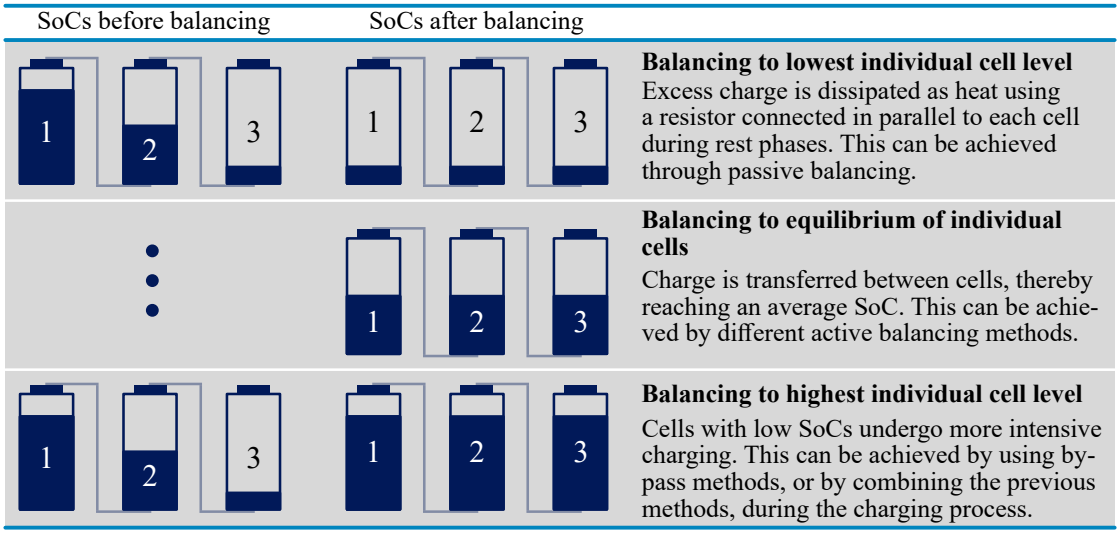

Figure 5. Balancing methods for battery packs

Balancing methods for serially connected cells, sorted by the SoC distribution achieved after balancing under the initial conditions specified in the first column. The resulting distribution can be a uniform SoC at the lowest, the highest, or an intermediate average value.

BATTERY STATES

Battery states, such as the SoC and SoH, are key to understanding battery performance and managing battery operation. At the cell level, they are defined by physico-chemical properties, such as lithium site occupancy, capacity, and resistance (see Note S2). However, in battery packs, cells can be in different states, making it impossible to define such quantities with the same physico-chemical significance. As a result, engineering definitions are required at the pack level, which may obscure differences between individual cells. For control and diagnostic purposes, engineering definitions of battery pack states are

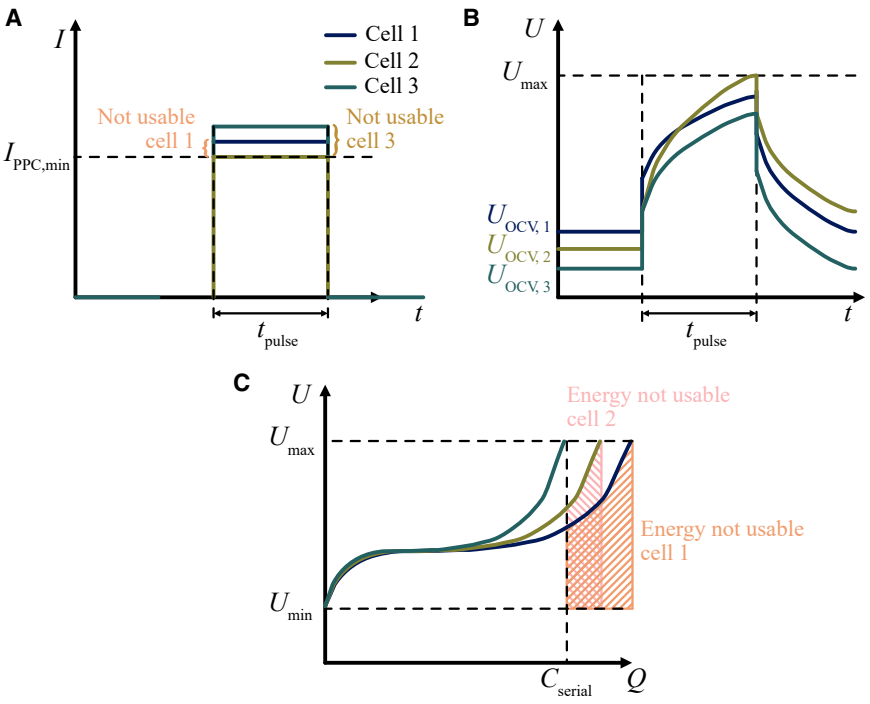

Figure 6. Schematic diagrams for calculating the pulse-power capability and total energy in serially connected lithium-ion batteries

(A and B) Schematic representation of the determination of the limiting current in the pulse test for three distinct cells (A) and the voltage response of those cells upon applying $I_{PPC,min}$ to the series connection (B).

(C) Voltage response of the three cells for a constant current charging and a maximum pack capacity of C_{serial}.

Table 2. Definitions of pack-state variables

Term	Definition	Reference
State of charge	$SoC_{pack} \triangleq \frac{\min_i\{SoC_i \cdot C_i\}}{C_{pack}}$	Li et al.,[64] Zhang et al.,[65] Zhong et al.,[55] Hua et al.,[52] Truchot et al.[66]
State of energy	$SoE_{pack} \triangleq \frac{Q\sum_i^{n_s}\int_{SoC_{start}}^{SoC_{end}} U_i(SoC)\mathrm{d}SoC}{C_{pack}\sum_i^{n_s}\int_{SoC_{pack}=0}^{SoC_{pack}=1} U_i(SoC)\mathrm{d}SoC}$	An et al.[67,68]
State of power	$SoP_{pack} \triangleq \frac{PPC_{serial}}{PPC_{serial,max}}$	–
Capacity-based state of health	$SoH_{C,pack} \triangleq \frac{C_{pack}}{C_{pack,BoL}}$	Su et al.,[69] Cordoba-Arenas et al.,[70] Sarmah et al.[71]
Capacity-based state of health, EoL bounded	$SoH_{C,pack,EoL} \triangleq \frac{C_{pack} - C_{pack,EoL}}{C_{pack,BoL} - C_{pack,EoL}}$	–
Resistance-based state of health	$SoH_{R,pack} \triangleq \frac{R_{pack}}{R_{pack,BoL}}$	Su et al.,[69] Cordoba-Arenas et al.[70]
Corrected resistance-based state of health	$SoH_{R,pack} \triangleq \frac{R_{pack,BoL}}{R_{pack}}$	–
Resistance-based state of health, EoL bounded	$SoH_{R,pack,EoL} \triangleq \frac{R_{pack,EoL} - R_{pack}}{R_{pack,EoL} - R_{pack,BoL}}$	–
Energy-based state of health	$SoH_{E,pack} \triangleq \frac{E_{pack}}{E_{pack,BoL}}$	Su et al.,[69] Diao et al.,[72] Chang et al.,[73] Zhang et al.[74]
Energy-based state of health, EoL bounded	$SoH_{E,pack} \triangleq \frac{E_{pack} - E_{pack,EoL}}{E_{pack,BoL} - E_{pack,EoL}}$	–

Pack-state variables for the serial connection of $i \in [1 \ldots n_s]$ (logical) cells. Definitions without a reference are newly introduced in this review.

typically used for series connections, which allow direct aggregation of voltage and current, while parallel groups are treated as logical cells. These states are typically defined on a scale from 0 to 1, where 0 represents an empty or degraded condition and 1 corresponds to a full or healthy state. Table 2 provides an overview of the relevant definitions.

Individual cells in a series connection typically exhibit different SoCs and capacities, leading to unusable capacity, as shown in Figure 7. Therefore, a definition that accounts for both quantities is required for the pack-level SoC_{pack}. Since a physical basis for SoC_{pack} does not exist, engineering definitions have been developed for different applications. The definition encountered most frequently is the ratio of the minimum dischargeable capacity to the pack capacity.[52,53,55,65] An issue with this definition occurs in the extreme scenario in which a pack contains cells at both 0% and 100% SoCs. In this case, the equation results in the indeterminate form 0/0, rendering the pack SoC undefined. This reflects the fact that such a pack cannot store usable charge and underscores the inherent difference between cell-level and pack-level states.

The SoE of a battery pack, SoE_{pack}, as defined by An et al.,[67,68] is the ratio of the pack's discharge energy to its total energy. Consequently, this definition of pack SoE accounts for energy losses and depends on the load current profile during discharge.

The state of power SoP_{pack} is defined as the ratio of a battery pack's available PPC, PPC_{serial}, to its maximum achievable PPC, $PPC_{serial,max}$. It can be specified for either the charging or the discharging case. The maximum possible PPC is determined using

$$PPC_{serial,max} = \begin{cases} I_{PPC,max} \cdot \left(n_s \cdot (U_{max} - U_{min}) - I_{PPC,max} \sum_i^{n_s} R_{DC,i} \right), I_{PPC,max} > 0 \text{ (charge)} \\ I_{PPC,max} \cdot \left(n_s \cdot (U_{max} - U_{min}) + I_{PPC,max} \sum_i^{n_s} R_{DC,i} \right), I_{PPC,max} < 0 \text{ (discharge)} \end{cases} . \quad \text{(Equation 22)}$$

The capacity-based SoH $SoH_{C,\,pack}$ is the ratio of the present pack capacity to the capacity of the pack at the beginning of life (BoL), $C_{pack,BoL}$.[69] The pack capacity SoH may not decrease

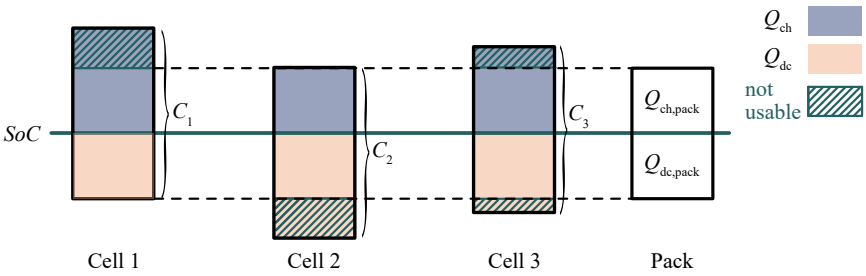

Figure 7. Battery pack capacity

Schematic representation of the determination of the battery pack discharge capacity, $Q_{dc,pack}$, and charge capacity, $Q_{ch,pack}$, for a series connection of 3 cells with varying individual discharge (Q_{dc}) and charge (Q_{ch}) capacities, as well as different SoCs. The shaded area indicates the unusable capacity of the individual cells.

monotonically because it depends on the overall pack capacity, which is influenced by SoC imbalances between cells. Since the degree of imbalance can fluctuate over time, increasing or decreasing, the pack capacity SoH may also vary accordingly. Furthermore, the $SoH_{C,\,pack}$ does not have a fixed range between 0 and 1, as the lower limit is never truly reached. To address this, we introduce the end-of-life (EoL)-bounded $SoH_{C,\,pack,EoL}$, which normalizes the pack capacity using its EoL capacity $C_{pack,EoL}$.

The resistance-based SoH $SoH_{R,pack}$ is the ratio of the present internal resistances of the pack R_{pack} to the internal resistance of the pack at the BoL $R_{pack,BoL}$. As the battery ages, the $SoH_{R,pack}$ increases monotonically with cell age, which contradicts the expected behavior of an SoH metric. SoH should decrease over the battery's lifetime and remain below its initial value of one at BoL. Therefore, this definition is unsuitable and needs to be rectified by using its reciprocal, which we define as the corrected resistance-based SoH. To ensure a bounded value range between 0 and 1 throughout the battery's service life, we introduce the EoL-bounded $SoH_{R,pack,EoL}$, which normalizes the pack resistance using its EoL capacity $R_{pack,EoL}$.

Finally, the energy-based SoH $SoH_{E,pack}$ is the ratio of the present pack energy E_{pack} to the energy of the pack at the BoL $E_{pack,BoL}$. The $SoH_{E,pack}$ accounts for imbalances between cells and does not necessarily decrease monotonically with cell aging, as variations in cell imbalances can cause fluctuations over time. Again, we define the EoL energy-based SoH as a normalized quantity, using the EoL energy of the battery pack as a reference.

To determine the previously described states, it is essential to collect information (e.g., resistances, capacitances, and SoCs) from individual cells. Note S3 outlines the most commonly used methods, which include single-cell analysis, the bar-delta method,[52,55,75–78] and the interval method.[64] However, these methods, as well as state estimation in general, are not the primary focus of this paper.

Inhomogeneities and uniqueness of pack states

The states of battery packs are not uniquely defined, as the same overall pack state can arise from different states of the individual cells. This ambiguity has significant implications for characterization, as the contributions of individual cells depend heavily on their specific states. Moreover, many pack-state descriptions rely on reference values (e.g., resistance, capacity, or energy) and defined operational windows.[79] Both vary significantly depending on the manufacturer,[80,81] the application,[82] and the specific cell or pack under investigation.[83] As a result, different characterization approaches may yield inconsistent outcomes for what is assumed to be the same pack state. To ensure reproducible characterization, providing a detailed and precise description of the pack's states is crucial.

In addition to specifying the (dis)charging profiles, it is essential to provide detailed information on the balancing procedure. Information on voltage ranges, reference values, and their determination must be clearly stated. The states and parameters of individual cells must be precisely defined. However, at this level of detail, the description can quickly become complex. We therefore propose first- and second-order state-difference descriptions, summarized in Table 3, as additional parameters for a more efficient comparison of results. While these descriptions offer a concise overview of the pack's condition, all information previously mentioned remains essential for reproducibility.

The first-order state-difference description quantifies the homogeneity between individual battery states and is therefore referred to as first-order state homogeneity. The SoC-based first-order state of homogeneity, $SoHo^{1st}_{SoC}$, quantifies the difference in SoCs among individual cells, providing a measure for balancing. Corresponding states can also be introduced to characterize aging effects. The unbounded-capacity-based first-order state of homogeneity $SoHo^{1st}_{C}$ represents the maximum capacity difference between individual cells relative to the maximum capacity. While the full range from 1 to 0 is theoretically possible, lower values are not practically relevant. Therefore, the EoL-bounded-capacity-based state of homogeneity $SoHo^{1st}_{C,EoL}$ is normalized to the capacity loss of the pack from BoL $C_{pack,BoL}$ to EoL $C_{pack,EoL}$.

The second-order state difference quantifies variations among individual cells by using the standard deviation, ensuring consistency in units with the measured quantity and enhancing interpretability. To determine these, the corresponding average values of the SoC (μ_{soc}), capacity (μ_C), and internal resistance (μ_R) of the individual cells are required. Unbounded definitions of the second-order state of homogeneity can be defined similarly. Alternatively, a state of inhomogeneity can be introduced, defined as $SoI = 1 - SoHo$.

In practice, we recommend using bounded state definitions ($SoX \in [0,1]$ with $X \in [C,E,P,H]$) together with state homogeneity metrics to ensure a clear, comparable, and application-relevant description of battery packs.

CHARACTERIZATION METHODS

Characterization methods such as electrochemical impedance spectroscopy (EIS), DRT analysis, pulse testing, and DVA,

Table 3. Definition of state-difference descriptions

Term	Definition
State-of-charge-based first-order state of homogeneity	$SoHo_{SoC}^{1st} \triangleq 1 - \max_{i \neq j}\{\lvert SoC_i - SoC_j \rvert\}$
Unbounded-capacity-based first-order state of homogeneity	$SoHo_{C}^{1st} \triangleq 1 - \frac{\max_{i \neq j}\{\lvert C_i - C_j \rvert\}}{\max\{C_i\}}$
EoL-bounded-capacity-based first-order state of homogeneity	$SoHo_{C,EoL}^{1st} \triangleq 1 - \frac{\max_{i \neq j}\{\lvert C_i - C_j \rvert\}}{C_{pack,BoL} - C_{pack,EoL}}$
Unbounded-resistance-based first-order state of homogeneity	$SoHo_{R}^{1st} \triangleq 1 - \frac{\max_{i \neq j}\{\lvert R_i - R_j \rvert\}}{\max_{i}\{R_i\}}$
EoL-bounded-resistance-based first-order state of homogeneity	$SoHo_{R,EoL}^{1st} \triangleq 1 - \frac{\max_{i \neq j}\{\lvert R_i - R_j \rvert\}}{n_s^{-1}(R_{pack,EoL} - R_{pack,BoL})}$
State-of-charge-based second-order state of homogeneity	$SoHo_{SoC}^{2nd} \triangleq 1 - n_s^{-1}\sqrt{\sum_{i=1}^{n_s}(SoC_i - \mu_{SoC})^2}$
Capacity-based second-order state of homogeneity	$SoHo_{C}^{2nd} \triangleq 1 - \frac{n_s^{-1}\sqrt{\sum_{i=1}^{n_s}(C_i - \mu_C)^2}}{C_{pack,BoL} - C_{pack,EoL}}$
Resistance-based second-order state of homogeneity	$SoHo_{R}^{2nd} \triangleq 1 - \frac{\sqrt{\sum_{i=1}^{n_s}(R_i - \mu_R)^2}}{R_{pack,EoL} - R_{pack,BoL}}$

First- and second-order states of homogeneity for a serial connection of $i \in [1 \ldots n_s]$ (logical) cells introduced in this review.

which were developed for electrodes and single cells, offer great potential for the diagnostics and characterization of battery packs and could enable a system-specific analysis of inhomogeneities and aging. In the context of electrical characterization, usually, a current signal is employed as the excitation, and a voltage response is utilized as the measurement. While it is technically possible to use cell-level characterization methods to study battery packs, meaningful and reliable results can only be obtained in conjunction with consistent pack-state definitions. The key is in combining cell- and pack-level information, including their inhomogeneities and variations, and understanding their interactions at the multi-component level. A physico-chemical interpretation of characterization results at the pack level is generally inadmissible and only helpful for discussion in conjunction with the state description of inhomogeneities.

In general, the electrical characterization can be carried out through a variety of methodologies, which are schematically illustrated in Figure 8. Wang et al.[84] distinguished between two approaches: centralized and distributed. In the centralized approach, the excitation signals are applied at the terminals of the entire pack, while in the distributed approach, these signals are individually applied to each (logical) cell. This distinction is extended to both excitation and measurement in this work. Furthermore, the centralized-distributed methodology is added. This approach simultaneously excites the entire pack while performing measurements on individual logical cells. However, this method necessitates precise synchronization between the excitation and measurement signals.

Among the available methodologies, the centralized approach holds a unique position: by analyzing only the terminal signals of the entire battery pack, it offers a simple and scalable solution that requires no access to individual cells, making it particularly attractive for real-world applications. While this allows for fast implementation, it also introduces fundamental limitations. Internal variations between cells—such as aging differences, defects, or outliers—are superimposed and effectively blurred. Consequently, global trends such as internal resistances can be tracked, but the interpretation remains qualitative. However, cell or pack failures, as well as inhomogeneous aging behavior, may still leave detectable signatures in the overall signal, offering potential for fast identification of outliers or unexpected pack behavior.

EIS

EIS is a widely recognized technique for analyzing electrochemical systems. Its primary objective is to determine the system's frequency response function, expressed as the complex impedance. By stimulating the system with a range of frequencies, specific electrochemical and transport processes—such as diffusion, migration through passivation layers, and charge transfer—can be selectively addressed and analyzed. Accurate results require the system to exhibit linear response behavior and remain time invariant, which necessitates the use of low-level signal amplitudes and strict validation protocols.[85–88] The methodology, along with numerous applications, is extensively covered in the literature, including textbooks[89] and review articles.[90–93]

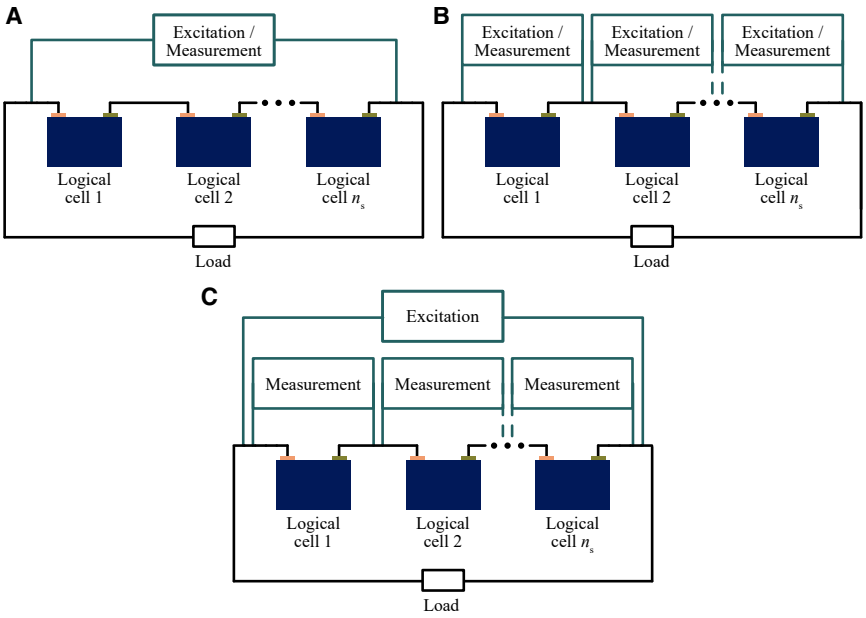

Figure 8. Schematic representation of different battery pack analysis methods
Centralized (A), distributed (B), and centralized-distributed (C) analyses of battery packs.

When applying EIS at the pack level, the parasitic effects of cell contacts, cable routing, and the battery management system can introduce both systematic and random errors in the impedance measurement.[94] Consequently, calibration is typically necessary to ensure accurate and reliable results, as demonstrated by Kasper et al.[95] However, additional challenges can arise depending on the connection topology.

In a parallel configuration, the lower impedance (cf. Figure 9A) leads to higher currents being required to maintain the same signal-to-noise ratio, creating significant challenges for the instrumentation. Moreover, measuring the current of individual cells is essential to verify the absence of balancing currents between them, as such currents can compromise the time invariance and linearity of the measurements. Given the potentially slow decay of balancing currents, future advancements may benefit from the application of nonlinear and time-varying methods.[96]

In a series connection, the effects vary depending on the analysis method employed. In a centralized approach, increasing the number of cells leads to greater impedance averaging, resulting in a loss of detailed information about individual cells[94,98] (cf. Figure 9B). This approach also presents challenges for measurement equipment, as high-precision voltage measurement is necessary to maintain a low current amplitude. Despite these challenges, EIS has been effectively applied in the centralized approach to identify inhomogeneously aged cells within a pack.[94,99]

In a distributed approach, the implementation and control of multiple switching devices can induce crosstalk between neighboring cells, potentially leading to inaccuracies in EIS measurements.[100] Beelen et al.[101] developed a method to account for crosstalk and subsequently applied it for temperature estimation. A review of different distributed devices and applications can be found in Wang et al.[84]

The centralized-distributed approach eliminates crosstalk and enables low-voltage measurements; however, synchronization between excitation and measurement remains a significant challenge. To the best of the authors' knowledge, no publications have yet been reported utilizing this approach.

DRT analysis

Identifying and separating the behavior of internal electrochemical processes using EIS alone is often challenging, which is why post-processing methods are frequently employed. One emerging technique for this purpose is DRT. This method deconvolves frequency-domain data into a time-domain distribution function, enhancing resolution and enabling the analysis of processes that would otherwise be difficult to separate. Due to the ill-posed and ill-conditioned nature of the DRT optimization problem, regularization is crucial for obtaining physically meaningful results. However, selecting an appropriate regularization parameter remains challenging,[102–105] and even with the correct parameter, some information may be lost due to peak merging and smoothing of the distribution function.[106] A detailed description of the method is available in the relevant literature[106–108] and review articles.[109–111]

To the best of the authors' knowledge, the DRT has been applied at the material and cell levels but has not yet been extended to the pack level.[109] Exploring pack-level integration is promising, as preliminary work on CtCvs[22] shows good results, and upscaling from the cell to the pack level may mirror effects seen in upscaling from half cells to full cells.

The potential of DRT on pack-level data strongly depends on the topology of the analysis. In the central approach, the smoothing effects of the regularization are superimposed on the CtCv and parasitic effects, which limit the interpretability of the results. In particular, this will complicate the identification of characteristics of individual cells. However, it may be feasible to determine the aging modes of the entire pack through a comparative analysis with a pack at the BoL.

The distributed and central-distributed approaches may enable the analysis of individual cells, but the success of this approach depends on data quality and parasitic effects, given the method's high sensitivity to measurement noise.[109,110] One potential solution is to use time-domain DRT[112–114] for analyzing pulse tests instead of impedance spectra. However, this approach may lead to the loss of high-frequency information due to limited sampling rates.

Pulse testing

Pulse tests apply charging or discharging pulses of constant current lasting several seconds, enabling characterization of a

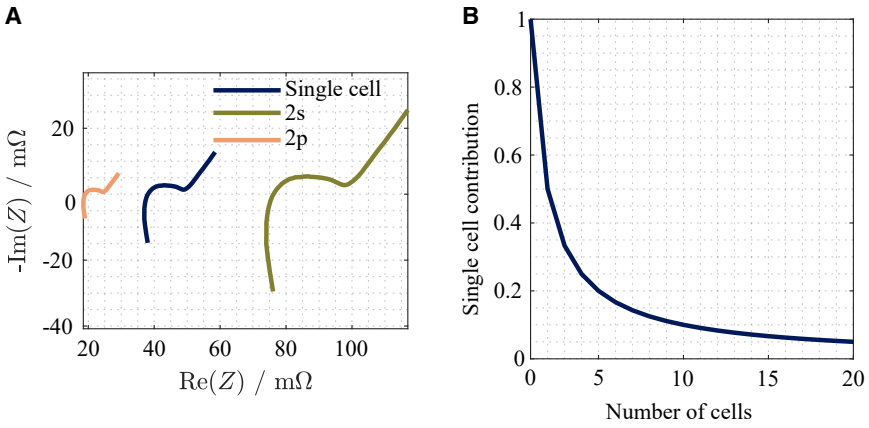

Figure 9. Impedance characteristics observed in battery pack application

Nyquist plot of impedance for a single cell, as well as for a series and a parallel connection of two cells from cell 1 of the dataset[97] (A) and the relative contribution of a single cell to the total impedance in a centralized approach with varying numbers of serially connected (logical) cells (B).

battery's internal resistance, dynamic response, and performance under realistic operating conditions. The hybrid pulse-power characterization test, introduced in EV battery test standards,[115] has become widely adopted.[116,117] While most standards use these tests to calculate pseudoresistance, the test is also used to parameterize equivalent-circuit models by analyzing voltage under load[118] or during relaxation.[22,119,120] The closely related galvanostatic intermittent titration technique uses a simplified diffusion model[121] to estimate diffusion coefficients, which, while non-transferable between cells,[122] reveal the impact of factors like SoC and temperature.[123] Specialized pulse tests with millisecond duration can measure true ohmic resistance,[124,125] often missed by standard equipment due to the overlap of time constants. Recent studies analyze pulse shapes at high sampling rates (>1 kHz) using Fourier transforms, linking the method to EIS.[126] However, translating results between time- and frequency-domain methods in nonlinear systems requires careful handling.[127]

Pulse testing can easily be applied to battery packs to determine total resistance or equivalent circuit model parameters.[53,128] Similar to EIS, individual cell characteristics are averaged, time constants are blurred, and additional impedance from cell connectors and wiring is incorporated.[129] In parallel connections, uneven current distribution requires modules with specially designed single current sensors,[11] limiting the method's applicability to highly integrated battery packs.

In the context of serial connections, the centralized-distributed approach facilitates the identification of production variations, temperature inhomogeneities, and intra-package aging variations,[19] during end-of-line testing, quick SoH assessment,[130] or during operation[127,131] through battery management electronics. Sampling rates above 100 Hz and precise synchronization between cell voltage and precise synchronization between cell voltage and current measurements are essential for this approach,[132] but recent advancements in modern application-specific integrated circuits have successfully addressed these challenges. For very large battery systems comprising thousands of cells, statistical methods for cell analysis are imperative.[133]

Integrating pulse tests during normal battery operation provides a future alternative to online EIS measurements, either by cell-individual excitation in a distributed approach, e.g., utilizing the cell-balancing circuitry,[134] or by utilizing chargers as free pulse sources in a centralized-distributed system.[135] However, current research primarily focuses on interpreting measurement results, with the main challenge being the separation of influencing factors such as temperature, SoC, and SoH.

Electrochemical voltage analysis

Incremental capacity analysis (ICA) and DVA are widely used techniques for diagnosing aging mechanisms and identifying specific degradation pathways in LIBs.[136,137] Both methods are based on the voltage response during charging and discharging, utilizing the first derivative of charge throughput $\partial Q \cdot \partial V^{-1} = f(V)$[138,139] and the voltage $\partial V \cdot \partial Q^{-1} = f(Q)$[140,141] for ICA and DVA respectively. This amplifies subtle voltage changes and, when combined with pre- and post-degradation data, provides a comprehensive assessment of active degradation modes.[136,142] A complete history and theoretical background for the techniques can be found in Barai et al.,[143] whereas Dubarry and Anseán[142] provide best practices for implementing them.

Performing ICA or DVA on packs with distributed or centralized-distributed monitoring is straightforward due to the availability of single-cell data. At the centralized level, IC and DV curves have been documented for packs since the late 2000s,[98,144–147] with studies comparing responses at the cell and pack levels.[42,80,81,83,148–152] These studies demonstrate a characteristic broadening of voltage features as the scale increases, as shown in Figures 10A and 10B. While voltage changes at the homogeneous single-cell level are well understood,[142] quantifying the impact of inhomogeneities remains challenging, both for single cells[18,140,153,154] and packs.[23,133] To predict these variations, pack models need to go beyond a simple scaled-up single-cell approach. They should allow separate degradation simulations for each cell, considering CtCv, imbalance, and balance, which is an inherently complex task. Accurate simulations of degradation and CtCv facilitate the modeling of the effects of imbalance due to the fact that the capacity and voltage response of each cell are known and can be used to estimate imbalances. Experimentally, quantifying this can be challenging, but methods have been proposed, such as using resting cell voltages[155] or graphical approaches.[156,157] The knowledge of each cell's voltage response and matching facilitates the simulation of balancing effects by applying one of several available balancing algorithms.[158]

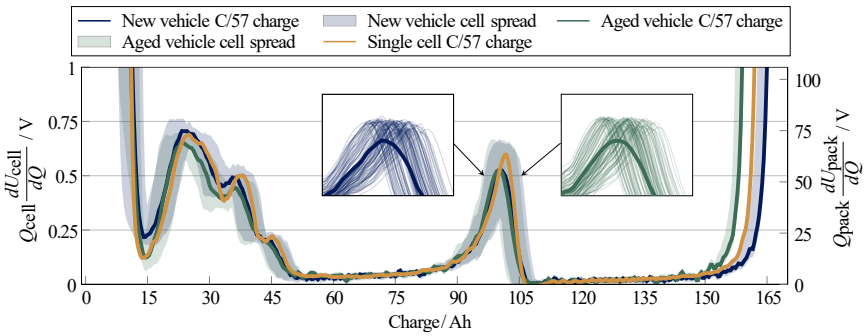

Figure 10. Differential voltage characteristics observed in battery pack application

Differential voltage curve for the cell spread at the BoL and EoL. The figure is revised from Rosenberger et al.[80]

While electrochemical voltage analyses are attractive and gaining traction for battery-management systems and pack applications, some hurdles remain for accurate diagnosis, especially for centralized monitoring. Most studies in the literature use high-resolution constant-current data over the entire voltage window, which might be complicated in deployed applications or if there is a significant imbalance without access to the single cells. However, recent work showcased that the technique can be used effectively outside of the constant current, using rest periods[133,159] or cases where the duty cycle is predictable.[160,161] Moreover, the use of a degradation-mode mechanistic model to generate synthetic data enveloping all degradations[162,163] or inhomogeneity levels[153,155] might offer the opportunity to test the applicability of any diagnosis approach on partial or noisier charge and discharge curves.[164] In addition, some further voltage and performance variations will also arise at the pack level because of inhomogeneities[18] induced by CtCvs, imbalance, and balancing.[158,165–169] interpretation at the pack level is complicated by CtCvs, parasitic effects, and non-uniform states. While the methods themselves are largely transferable, their diagnostic value depends critically on an accurate description and understanding of the battery pack and its states. Due to the superposition of heterogeneous cell responses, pack-level characterization does not reflect distinct electrochemical processes as clearly as at the single-cell level. Instead, characteristic features are averaged, broadened, or masked, limiting analysis to qualitative trends rather than allowing quantitative or mechanistic interpretation. To enable reliable application and to raise the method's potential at the pack level, further detailed work is required to account for interconnect topology, current distribution, and analysis configuration (e.g., centralized vs. distributed), as these factors significantly influence both signal quality and interpretability of the results.

The main conclusion of this work is that meaningful and reliable characterization of battery packs requires the combined application of adapted characterization methods and harmonized and unambiguously defined pack-level states. Bridging this gap will enable robust monitoring, accurate diagnostics, predictive maintenance, and reliable operation of battery packs.

This review sheds light on a rapidly evolving research field marked by significant challenges. It achieves two key goals: consolidating fragmented knowledge and bridging critical gaps, thereby laying the foundation for progress in both scientific understanding and real-world applications such as e-mobility and grid-scale energy storage.

OVERVIEW AND OUTLOOK

This review consolidates the fundamental principles of the electrical and electrochemical properties and behavior of battery packs, addressing fragmented knowledge to provide a foundation for future research.

Two major challenges are identified. First, the lack of harmonized definitions for key battery states, such as SoC, SoE, and SoH, hampers the interpretation of pack-level characterization results, as well as the comparability and reproducibility of results across studies. To address this, we provide a structured review of existing definitions, suggest adaptations, introduce new state definitions, and provide informed recommendations on the most appropriate definitions for consistent and meaningful application. However, state definitions at the pack level remain ambiguous, as the same overall pack state can result from different combinations of individual cell states. To address this, we introduce the state of homogeneity as an additional descriptor that allows for a more accurate and comprehensive description of battery packs.

The second challenge is the characterization of battery packs. The core difficulty here is not the availability of methods but their meaningful application to multi-component systems. Many techniques, such as EIS, DRT, pulse testing, and electrochemical voltage analysis, are well established at the cell level, but their

ACKNOWLEDGMENTS

This work was partially supported by the Office of Naval Research (N00014-22-1-2045) through funding provided to M.D. and by the German Federal Ministry of Education and Research (BMBF) within the project "TUBE" (03XP0425) through funding provided to J.S.

AUTHOR CONTRIBUTIONS

Conceptualization, T.R. and M.A.D.; data curation, T.R.; formal analysis, T.R., W.H., M.S.T., G.L.P., M.D., N.K., J.M., F.R., A.J., J.S., M.L., O.B., and M.A.D.; methodology, T.R. and M.A.D.; visualization, T.R., W.H., M.S.T., G.L.P., M.D., F.R., A.J., J.S., and M.L.; writing – original draft, T.R., W.H., M.S.T., G.L.P., M. D., N.K., J.M., F.R., A.J., J.S., M.L., O.B., and M.A.D.; writing – review & editing, T.R., W.H., M.S.T., G.L.P., M.D., N.K., J.M., F.R., A.J., J.S., M.L., O.B., and M.A.D.

DECLARATION OF INTERESTS

The authors declare no competing interests.

DECLARATION OF GENERATIVE AI AND AI-ASSISTED TECHNOLOGIES IN THE WRITING PROCESS

During the preparation of this work, the authors used ChatGPT by OpenAI and Writer by DeepL to improve the language of the manuscript. After using this tool or service, the authors reviewed and edited the content as needed and take full responsibility for the content of the publication.

SUPPLEMENTAL INFORMATION

Supplemental information can be found online at https://doi.org/10.1016/j.xcrp.2025.102919.

REFERENCES

1. Fleischmann, J., Hanicke, M., Horetsky, E., Ibrahim, D., Jautelat, S., Linder, M., Schaufuss, P., Torscht, L., and van de Rijt, A. (2023). Battery 2030: Resilient, sustainable, and circular. McKinsey & Company *16*, 2023.
2. Gersdorf, T., Hertzke, P., Schaufuss, P., and Schenk, S. (2020). McKinsey Electric Vehicle Index: Europe cushions a global plunge in EV sales. https://www.mckinsey.com/industries/automotive-and-assembly/our-insights/mckinsey-electric-vehicle-index-europe-cushions-a-global-plunge-in-ev-sales#/.
3. Rostami, H., Valio, J., Suominen, P., Tynjälä, P., and Lassi, U. (2024). Advancements in cathode technology, recycling strategies, and market dynamics: A comprehensive review of sodium ion batteries. Chem. Eng. J. *495*, 153471. https://doi.org/10.1016/j.cej.2024.153471.
4. Plett, G.L. (2016). Battery Management Systems 2 of Artech House Power Engineering and Power Electronics (Boston: Artech House).
5. Jossen, A., and Weydanz, W. (2021). Moderne Akkumulatoren richtig einsetzen. In: 2. überarbeitete auflage, unverändert zur 2. auflage vom februar 2019 (MatrixMedia Verlag).
6. Liu, X., Ai, W., Naylor Marlow, M., Patel, Y., and Wu, B. (2019). The effect of cell-to-cell variations and thermal gradients on the performance and degradation of lithium-ion battery packs. Appl. Energy *248*, 489–499. https://doi.org/10.1016/j.apenergy.2019.04.108.
7. Baumhöfer, T., Brühl, M., Rothgang, S., and Sauer, D.U. (2014). Production caused variation in capacity aging trend and correlation to initial cell performance. J. Power Sources *247*, 332–338. https://doi.org/10.1016/j.jpowsour.2013.08.108.
8. Harris, S.J., Harris, D.J., and Li, C. (2017). Failure statistics for commercial lithium ion batteries: A study of 24 pouch cells. J. Power Sources *342*, 589–597. https://doi.org/10.1016/j.jpowsour.2016.12.083.
9. Laue, V., Schmidt, O., Dreger, H., Xie, X., Röder, F., Schenkendorf, R., Kwade, A., and Krewer, U. (2020). Model–Based Uncertainty Quantification for the Product Properties of Lithium–Ion Batteries. Energy Technol. *8*, 201900201. https://doi.org/10.1002/ente.201900201.
10. Rumpf, K., Naumann, M., and Jossen, A. (2017). Experimental investigation of parametric cell-to-cell variation and correlation based on 1100 commercial lithium-ion cells. J. Energy Storage *14*, 224–243. https://doi.org/10.1016/j.est.2017.09.010.
11. Brand, M.J., Hofmann, M.H., Steinhardt, M., Schuster, S.F., and Jossen, A. (2016). Current distribution within parallel-connected battery cells. J. Power Sources *334*, 202–212. https://doi.org/10.1016/j.jpowsour.2016.10.010.
12. Song, Z., Yang, N., Lin, X., Pinto Delgado, F., Hofmann, H., and Sun, J. (2022). Progression of cell-to-cell variation within battery modules under different cooling structures. Appl. Energy *312*, 118836. https://doi.org/10.1016/j.apenergy.2022.118836.
13. Gogoana, R., Pinson, M.B., Bazant, M.Z., and Sarma, S.E. (2014). Internal resistance matching for parallel-connected lithium-ion cells and impacts on battery pack cycle life. J. Power Sources *252*, 8–13. https://doi.org/10.1016/j.jpowsour.2013.11.101.
14. Offer, G.J., Yufit, V., Howey, D.A., Wu, B., and Brandon, N.P. (2012). Module design and fault diagnosis in electric vehicle batteries. J. Power Sources *206*, 383–392. https://doi.org/10.1016/j.jpowsour.2012.01.087.
15. Yang, N., Zhang, X., Shang, B., and Li, G. (2016). Unbalanced discharging and aging due to temperature differences among the cells in a lithium-ion battery pack with parallel combination. J. Power Sources *306*, 733–741. https://doi.org/10.1016/j.jpowsour.2015.12.079.
16. Paul, S., Diegelmann, C., Kabza, H., and Tillmetz, W. (2013). Analysis of ageing inhomogeneities in lithium-ion battery systems. J. Power Sources *239*, 642–650. https://doi.org/10.1016/j.jpowsour.2013.01.068.
17. Bruen, T., and Marco, J. (2016). Modelling and experimental evaluation of parallel connected lithium ion cells for an electric vehicle battery system. J. Power Sources *310*, 91–101. https://doi.org/10.1016/j.jpowsour.2016.01.001.
18. Beck, D., Dechent, P., Junker, M., Sauer, D.U., and Dubarry, M. (2021). Inhomogeneities and Cell-to-Cell Variations in Lithium-Ion Batteries, a Review. Energies *14*, 3276. https://doi.org/10.3390/en14113276.
19. Dubarry, M., Vuillaume, N., and Liaw, B.Y. (2010). Origins and accommodation of cell variations in Li-ion battery pack modeling. Int. J. Energy Res. *34*, 216–231. https://doi.org/10.1002/er.1668.
20. Schuster, S.F., Brand, M.J., Berg, P., Gleissenberger, M., and Jossen, A. (2015). Lithium-ion cell-to-cell variation during battery electric vehicle operation. J. Power Sources *297*, 242–251. https://doi.org/10.1016/j.jpowsour.2015.08.001.
21. An, F., Chen, L., Huang, J., Zhang, J., and Li, P. (2016). Rate dependence of cell-to-cell variations of lithium-ion cells. Sci. Rep. *6*, 35051. https://doi.org/10.1038/srep35051.
22. Rüther, T., Schamel, M., Plank, C., Schomburg, F., Röder, F., and Danzer, M.A. (2023). Cell-to-cell variation beyond parameter analysis — Identification and correlation of processes in Lithium-Ion Batteries using a combined distribution of relaxation times analysis. J. Power Sources *587*, 233677. https://doi.org/10.1016/j.jpowsour.2023.233677.
23. Dubarry, M., Pastor-Fernández, C., Baure, G., Yu, T.F., Widanage, W.D., and Marco, J. (2019). Battery energy storage system modeling: Investigation of intrinsic cell-to-cell variations. J. Energy Storage *23*, 19–28. https://doi.org/10.1016/j.est.2019.02.016.
24. Luan, C., Ma, C., Wang, C., Chang, L., Xiao, L., Yu, Z., and Li, H. (2021). Influence of the connection topology on the performance of lithium-ion battery pack under cell-to-cell parameters variations. J. Energy Storage *41*, 102896. https://doi.org/10.1016/j.est.2021.102896.
25. Porpora, F., D'Arpino, M., Cheng, Y., Rizzoni, G., and Tomasso, G. (2023). Reduced Order Model of Common Battery Pack Architectures for Assessment of Cell Parameter Variation Propagation. IEEE Access *11*, 96693–96709. https://doi.org/10.1109/ACCESS.2023.3312236.
26. Kim, K., and Choi, J.I. (2023). Effect of cell-to-cell variation and module configuration on the performance of lithium-ion battery systems. Appl. Energy *352*, 121888. https://doi.org/10.1016/j.apenergy.2023.121888.
27. Lingzhao, K., and Lee, R. (2021). A Study on Parameter Variation of Cells Effects on Battery Groups with Different Topologies and Load Profiles. SAE Int. J. Adv. Curr. Pract. Mobil. *3*, 2770–2781. https://doi.org/10.4271/2021-01-0756.
28. Tangmongkhonsuk, J., Fuengwarodsakul, N.H., Kerdsup, B., and Masomtob, M. (2024). (5272024). Study on Effect of Terminal Placement in Low Voltage Li-Ion 18650 Battery Pack. In 21st International Conference on Electrical Engineering/Electronics, Computer, Telecommunications and Information Technology (ECTI-CON) (IEEE), pp. 1–6. https://doi.org/10.1109/ECTI-CON60892.2024.10594910.
29. Schindler, M., Durdel, A., Sturm, J., Jocher, P., and Jossen, A. (2020). On the Impact of Internal Cross-Linking and Connection Properties on the Current Distribution in Lithium-Ion Battery Modules. J. Electrochem. Soc. *167*, 120542. https://doi.org/10.1149/1945-7111/abad6b.

30. Zwicker, M.F.R., Moghadam, M., Zhang, W., and Nielsen, C.V. (2020). Automotive battery pack manufacturing – a review of battery to tab joining. Journal of Advanced Joining Processes *1*, 100017. https://doi.org/10.1016/j.jajp.2020.100017.

31. Kumar, N., Pamarthi, V.V., Harris, C., Burbidge, E., and Masters, I. (2024). Dual-mode laser beam welding of similar and dissimilar material tab-to-busbar for electric vehicle battery pack. Journal of Advanced Joining Processes *10*, 100250. https://doi.org/10.1016/j.jajp.2024.100250.

32. Kumar, N., Ramakrishnan, S.M., Panchapakesan, K., Subramaniam, D., Masters, I., Dowson, M., and Das, A. (2022). In-depth evaluation of micro-resistance spot welding for connecting tab to 18,650 Li-ion cells for electric vehicle battery application. Int. J. Adv. Manuf. Technol. *121*, 6581–6597. https://doi.org/10.1007/s00170-022-09775-z.

33. Das, A., Ashwin, T.R., and Barai, A. (2019). Modelling and characterisation of ultrasonic joints for Li-ion batteries to evaluate the impact on electrical resistance and temperature raise. J. Energy Storage *22*, 239–248. https://doi.org/10.1016/j.est.2019.02.017.

34. Brand, M.J., Schmidt, P.A., Zaeh, M.F., and Jossen, A. (2015). Welding techniques for battery cells and resulting electrical contact resistances. J. Energy Storage *1*, 7–14. https://doi.org/10.1016/j.est.2015.04.001.

35. H. Larsson, A. Chamberlain, S. Walin, S. Shouri, L. Nilsson, E. Myrsell, and D. Vasquez (2019). Welding methods for electrical connections in battery systems. (Uppsala Universitet).

36. Zhang, Q., Sekol, R.C., Zhang, C., Li, Y., and Carlson, B.E. (2019). Joining Lithium-Ion Battery Tabs Using Solder-Reinforced Adhesive. J. Manuf. Sci. Eng. *141*, 4042842. https://doi.org/10.1115/1.4042842.

37. Brand, M.J., Berg, P., Kolp, E.I., Bach, T., Schmidt, P., and Jossen, A. (2016). Detachable electrical connection of battery cells by press contacts. J. Energy Storage *8*, 69–77. https://doi.org/10.1016/j.est.2016.09.011.

38. Bolsinger, C., Zorn, M., and Birke, K.P. (2017). Electrical contact resistance measurements of clamped battery cell connectors for cylindrical 18650 battery cells. J. Energy Storage *12*, 29–36. https://doi.org/10.1016/j.est.2017.04.001.

39. Fu, R., Choe, S.Y., Jackson, R.L., Flowers, G.T., and Kim, D. (2012). Modeling and Analysis of Vibration-Induced Changes in Connector Resistance of High Power Electrical Connectors for Hybrid Vehicles. Mech. Base. Des. Struct. Mach. *40*, 349–365. https://doi.org/10.1080/15397734.2012.670098.

40. Elkjaer, A., Ringen, G., Bjørge, R., Musinoi Hagen, C.H., Lædre, S., and Magnusson, N. (2023). Reliability of Bolted Aluminum Busbars for Battery Systems: Effect of Nickel Coating and Corrosive Environment. IEEE Trans. Transp. Electrific. *9*, 1060–1071. https://doi.org/10.1109/TTE.2022.3196309.

41. Rothgang, S., Baumhöfer, T., van Hoek, H., Lange, T., de Doncker, R.W., and Sauer, D.U. (2015). Modular battery design for reliable, flexible and multi-technology energy storage systems. Appl. Energy *137*, 931–937. https://doi.org/10.1016/j.apenergy.2014.06.069.

42. Jocher, P., Roehrer, F., Rehm, M., Idrizi, T., Himmelreich, A., and Jossen, A. (2024). Scaling from cell to system: Comparing Lithium-ion and Sodium-ion technologies regarding inhomogeneous resistance and temperature in parallel configuration by sensitivity factors. J. Energy Storage *98*, 112931. https://doi.org/10.1016/j.est.2024.112931.

43. Roehrer, F., Jocher, P., Rehm, M., Graule, A., and Jossen, A. (2025). Real-time replication of battery cells using digital twins: A novel experimental methodology to measure current inhomogeneity in n-parallel configurations. J. Power Sources *640*, 236573. https://doi.org/10.1016/j.jpowsour.2025.236573.

44. Plett, G.L. (2004). Extended Kalman filtering for battery management systems of LiPB-based HEV battery packs. J. Power Sources *134*, 277–292. https://doi.org/10.1016/j.jpowsour.2004.02.033.

45. Gong, X., Xiong, R., and Mi, C.C. (2015). Study of the Characteristics of Battery Packs in Electric Vehicles With Parallel-Connected Lithium-Ion Battery Cells. IEEE Trans. Ind. Appl. *51*, 1872–1879. https://doi.org/10.1109/TIA.2014.2345951.

46. Fill, A., Koch, S., Pott, A., and Birke, K.P. (2018). Current distribution of parallel-connected cells in dependence of cell resistance, capacity and number of parallel cells. J. Power Sources *407*, 147–152. https://doi.org/10.1016/j.jpowsour.2018.10.061.

47. Fill, A., Koch, S., and Birke, K.P. (2019). Analytical model of the current distribution of parallel-connected battery cells and strings. J. Energy Storage *23*, 37–43. https://doi.org/10.1016/j.est.2019.02.031.

48. Hofmann, M.H., Czyrka, K., Brand, M.J., Steinhardt, M., Noel, A., Spingler, F.B., and Jossen, A. (2018). Dynamics of current distribution within battery cells connected in parallel. J. Energy Storage *20*, 120–133. https://doi.org/10.1016/j.est.2018.08.013.

49. Naylor Marlow, M., Chen, J., and Wu, B. (2024). Degradation in parallel-connected lithium-ion battery packs under thermal gradients. Commun. Eng. *3*, 00153. https://doi.org/10.1038/s44172-023-00153-5.

50. Rüwald, T., Marongiu, A., Chahardahcherik, D., van Faassen, H., Ditler, H., Schulte, D., and Figgemeier, E. (2024). Experimental investigation of cell degradation in packs of parallel-connected cells under different temperature distributions. J. Energy Storage *104*, 114427. https://doi.org/10.1016/j.est.2024.114427.

51. Schindler, M., Jocher, P., Durdel, A., and Jossen, A. (2021). Analyzing the Aging Behavior of Lithium-Ion Cells Connected in Parallel Considering Varying Charging Profiles and Initial Cell-to-Cell Variations. J. Electrochem. Soc. *168*, 090524. https://doi.org/10.1149/1945-7111/ac2089.

52. Hua, Y., Cordoba-Arenas, A., Warner, N., and Rizzoni, G. (2015). A multi time-scale state-of-charge and state-of-health estimation framework using nonlinear predictive filter for lithium-ion battery pack with passive balance control. J. Power Sources *280*, 293–312. https://doi.org/10.1016/j.jpowsour.2015.01.112.

53. Li, J., and Mazzola, M.S. (2013). Accurate battery pack modeling for automotive applications. J. Power Sources *237*, 215–228. https://doi.org/10.1016/j.jpowsour.2013.03.009.

54. Wang, X., Fang, Q., Dai, H., Chen, Q., and Wei, X. (2021). Investigation on Cell Performance and Inconsistency Evolution of Series and Parallel Lithium–Ion Battery Modules. Energy Technol. *9*, 202100072. https://doi.org/10.1002/ente.202100072.

55. Zhong, L., Zhang, C., He, Y., and Chen, Z. (2014). A method for the estimation of the battery pack state of charge based on in-pack cells uniformity analysis. Appl. Energy *113*, 558–564. https://doi.org/10.1016/j.apenergy.2013.08.008.

56. Plett, G.L. (2024). Review and some perspectives on different methods to estimate state of charge of lithium-ion batteries. Journal of Automotive Safety and Energy *3*, 001. https://doi.org/10.3969/j.issn.1674-8484.2019.03.001.

57. Omariba, Z.B., Zhang, L., and Sun, D. (2019). Review of Battery Cell Balancing Methodologies for Optimizing Battery Pack Performance in Electric Vehicles. IEEE Access *7*, 129335–129352. https://doi.org/10.1109/ACCESS.2019.2940090.

58. Wu, J.C., Jou, H.L., and Chuang, P.H. (2013). Voltage equaliser for Li–Fe battery. Int. J. Electron. *100*, 1398–1413. https://doi.org/10.1080/00207217.2012.743090.

59. Anderson, R.D., Zane, R., Plett, G., Maksimovic, D., Smith, K., and Trimboli, M.S. (2017). Life Balancing – A Better Way to Balance Large Batteries. In SAE Technical Paper Series. SAE Technical Paper Series. (SAE International). https://doi.org/10.4271/2017-01-1210.

60. Baronti, F., Roncella, R., and Saletti, R. (2014). Performance comparison of active balancing techniques for lithium-ion batteries. J. Power Sources *267*, 603–609. https://doi.org/10.1016/j.jpowsour.2014.05.007.

61. Cao, J., Schofield, N., and Emadi, A. (2008). Battery balancing methods: A comprehensive review. In 2008 IEEE Vehicle Power and

Propulsion Conference (IEEE), pp. 1–6. https://doi.org/10.1109/VPPC.2008.4677669.

62. Moore, S.W., and Schneider, P.J. (2001). A Review of Cell Equalization Methods for Lithium Ion and Lithium Polymer Battery Systems. In SAE Technical Paper Series. SAE Technical Paper Series (SAE International). https://doi.org/10.4271/2001-01-0959.

63. Khan, N., Ooi, C.A., Alturki, A., Amir, M., Alharbi, T., and Alharbi, T. (2024). A critical review of battery cell balancing techniques, optimal design, converter topologies, and performance evaluation for optimizing storage system in electric vehicles. Energy Rep. *11*, 4999–5032. https://doi.org/10.1016/j.egyr.2024.04.041.

64. Li, J., Greye, B., Buchholz, M., and Danzer, M.A. (2017). Interval method for an efficient state of charge and capacity estimation of multicell batteries. J. Energy Storage *13*, 1–9. https://doi.org/10.1016/j.est.2017.05.012.

65. Zhang, X., Wang, Y., Yang, D., and Chen, Z. (2016). An on-line estimation of battery pack parameters and state-of-charge using dual filters based on pack model. Energy *115*, 219–229. https://doi.org/10.1016/j.energy.2016.08.109.

66. Truchot, C., Dubarry, M., and Liaw, B.Y. (2014). State-of-charge estimation and uncertainty for lithium-ion battery strings. Appl. Energy *119*, 218–227. https://doi.org/10.1016/j.apenergy.2013.12.046.

67. An, F., Jiang, J., Zhang, W., Zhang, C., and Fan, X. (2022). State of Energy Estimation for Lithium-Ion Battery Pack via Prediction in Electric Vehicle Applications. IEEE Trans. Veh. Technol. *71*, 184–195. https://doi.org/10.1109/TVT.2021.3125194.

68. An, F., Zhang, W., Sun, B., Jiang, J., and Fan, X. (2023). A novel state-of-energy simplified estimation method for lithium-ion battery pack based on prediction and representative cells. J. Energy Storage *63*, 107083. https://doi.org/10.1016/j.est.2023.107083.

69. Su, L., Xu, Y., and Dong, Z. (2024). State–of–health estimation of lithium–ion batteries: A comprehensive literature review from cell to pack levels. Energy Conversion and Econom. *5*, 224–242. https://doi.org/10.1049/enc2.12125.

70. Cordoba-Arenas, A., Onori, S., and Rizzoni, G. (2015). A control-oriented lithium-ion battery pack model for plug-in hybrid electric vehicle cycle-life studies and system design with consideration of health management. J. Power Sources *279*, 791–808. https://doi.org/10.1016/j.jpowsour.2014.12.048.

71. Sarmah, S.B., Kalita, P., Garg, A., Niu, X.d., Zhang, X.W., Peng, X., and Bhattacharjee, D. (2019). A Review of State of Health Estimation of Energy Storage Systems: Challenges and Possible Solutions for Futuristic Applications of Li-Ion Battery Packs in Electric Vehicles. Journal of Electrochemical Energy Conversion and Storage *16*, 4042987. https://doi.org/10.1115/1.4042987.

72. Diao, W., Jiang, J., Zhang, C., Liang, H., and Pecht, M. (2017). Energy state of health estimation for battery packs based on the degradation and inconsistency. Energy Proc. *142*, 3578–3583. https://doi.org/10.1016/j.egypro.2017.12.248.

73. Chang, C., Wu, Y., Jiang, J., Jiang, Y., Tian, A., Li, T., and Gao, Y. (2022). Prognostics of the state of health for lithium-ion battery packs in energy storage applications. Energy *239*, 122189. https://doi.org/10.1016/j.energy.2021.122189.

74. Zhang, X., Wang, Y., Liu, C., and Chen, Z. (2018). A novel approach of battery pack state of health estimation using artificial intelligence optimization algorithm. J. Power Sources *376*, 191–199. https://doi.org/10.1016/j.jpowsour.2017.11.068.

75. Dai, H., Wei, X., Sun, Z., Wang, J., and Gu, W. (2012). Online cell SOC estimation of Li-ion battery packs using a dual time-scale Kalman filtering for EV applications. Appl. Energy *95*, 227–237. https://doi.org/10.1016/j.apenergy.2012.02.044.

76. Plett, G.L.. Efficient Battery Pack State Estimation using Bar-Delta Filtering. EVS24. http://mocha-java.uccs.edu/dossier/RESEARCH/2009evs24c-.pdf.

77. Sun, F., and Xiong, R. (2015). A novel dual-scale cell state-of-charge estimation approach for series-connected battery pack used in electric vehicles. J. Power Sources *274*, 582–594. https://doi.org/10.1016/j.jpowsour.2014.10.119.

78. Zheng, Y., Ouyang, M., Lu, L., Li, J., Han, X., Xu, L., Ma, H., Dollmeyer, T. A., and Freyermuth, V. (2013). Cell state-of-charge inconsistency estimation for LiFePO4 battery pack in hybrid electric vehicles using mean-difference model. Appl. Energy *111*, 571–580. https://doi.org/10.1016/j.apenergy.2013.05.048.

79. Hu, X., Feng, F., Liu, K., Zhang, L., Xie, J., and Liu, B. (2019). State estimation for advanced battery management: Key challenges and future trends. Renew. Sustain. Energy Rev. *114*, 109334. https://doi.org/10.1016/j.rser.2019.109334.

80. Rosenberger, N., Rosner, P., Bilfinger, P., Schöberl, J., Teichert, O., Schneider, J., Abo Gamra, K., Allgäuer, C., Dietermann, B., Schreiber, M., et al. (2024). Quantifying the State of the Art of Electric Powertrains in Battery Electric Vehicles: Comprehensive Analysis of the Tesla Model 3 on the Vehicle Level. World Electric Vehicle Journal *15*, 15060268. https://doi.org/10.3390/wevj15060268.

81. Wassiliadis, N., Steinsträter, M., Schreiber, M., Rosner, P., Nicoletti, L., Schmid, F., Ank, M., Teichert, O., Wildfeuer, L., Schneider, J., et al. (2022). Quantifying the state of the art of electric powertrains in battery electric vehicles: Range, efficiency, and lifetime from component to system level of the Volkswagen ID.3. eTransportation *12*, 100167. https://doi.org/10.1016/j.etran.2022.100167.

82. Collath, N., Tepe, B., Englberger, S., Jossen, A., and Hesse, H. (2022). Aging aware operation of lithium-ion battery energy storage systems: A review. J. Energy Storage *55*, 105634. https://doi.org/10.1016/j.est.2022.105634.

83. Bilfinger, P., Rosner, P., Schreiber, M., Kröger, T., Gamra, K.A., Ank, M., Wassiliadis, N., Dietermann, B., and Lienkamp, M. (2024). Battery pack diagnostics for electric vehicles: Transfer of differential voltage and incremental capacity analysis from cell to vehicle level. eTransportation *22*, 100356. https://doi.org/10.1016/j.etran.2024.100356.

84. Wang, X., Wei, X., Zhu, J., Dai, H., Zheng, Y., Xu, X., and Chen, Q. (2021). A review of modeling, acquisition, and application of lithium-ion battery impedance for onboard battery management. eTransportation *7*, 100093. https://doi.org/10.1016/j.etran.2020.100093.

85. Plank, C., Ruther, T., and Danzer, M.A. (2022). (9272022). Detection of Non-Linearity and Non-Stationarity in Impedance Spectra using an Extended Kramers-Kronig Test without Overfitting. In International Workshop on Impedance Spectroscopy (IWIS) (IEEE), pp. 1–6. https://doi.org/10.1109/IWIS57888.2022.9975131.

86. Yrjänä, V., and Bobacka, J. (2024). Methods for automating and improving the robustness of linear Kramers–Kronig tests for the purposes of validating immittance spectra. Electrochim. Acta *504*, 144951. https://doi.org/10.1016/j.electacta.2024.144951.

87. Boukamp, B.A. (1995). A Linear Kronig–Kramers Transform Test for Immittance Data Validation. J. Electrochem. Soc. *142*, 1885–1894. https://doi.org/10.1149/1.2044210.

88. Kasper, M., Leike, A., Thielmann, J., Winkler, C., Al-Zubaidi R-Smith, N., and Kienberger, F. (2022). Electrochemical impedance spectroscopy error analysis and round robin on dummy cells and lithium-ion-batteries. J. Power Sources *536*, 231407. https://doi.org/10.1016/j.jpowsour.2022.231407.

89. Barsoukov, E. (2005). Impedance Spectroscopy: Theory, Experiment, and Applications (Hoboken: John Wiley & Sons Incorporated).

90. Wang, S., Zhang, J., Gharbi, O., Vivier, V., Gao, M., and Orazem, M.E. (2021). Electrochemical impedance spectroscopy. Nat. Rev. Methods Primers *1*, 41. https://doi.org/10.1038/s43586-021-00039-w.

91. Vadhva, P., Hu, J., Johnson, M.J., Stocker, R., Braglia, M., Brett, D.J.L., and Rettie, A.J.E. (2021). Electrochemical Impedance Spectroscopy for All–Solid–State Batteries: Theory, Methods and Future Outlook. Chemelectrochem *8*, 1930–1947. https://doi.org/10.1002/celc.202100108.

92. Iurilli, P., Brivio, C., and Wood, V. (2021). On the use of electrochemical impedance spectroscopy to characterize and model the aging phenomena of lithium-ion batteries: a critical review. J. Power Sources *505*, 229860. https://doi.org/10.1016/j.jpowsour.2021.229860.

93. Meddings, N., Heinrich, M., Overney, F., Lee, J.S., Ruiz, V., Napolitano, E., Seitz, S., Hinds, G., Raccichini, R., Gaberšček, M., and Park, J. (2020). Application of electrochemical impedance spectroscopy to commercial Li-ion cells: A review. J. Power Sources *480*, 228742. https://doi.org/10.1016/j.jpowsour.2020.228742.

94. Rüther, T., Plank, C., Schamel, M., and Danzer, M.A. (2023). Detection of inhomogeneities in serially connected lithium-ion batteries. Appl. Energy *332*, 120514. https://doi.org/10.1016/j.apenergy.2022.120514.

95. Kasper, M., Moertelmaier, M., Ragulskis, M., Al–Zubaidi R–Smith, N., Angerer, J., Aufreiter, M., Romero, A., Krummacher, J., Xu, J., Root, D.E., and Kienberger, F. (2023). Calibrated Electrochemical Impedance Spectroscopy and Time–Domain Measurements of a 7 kWh Automotive Lithium–Ion Battery Module with 396 Cylindrical Cells. Batteries & Supercaps *6*, 202200415. https://doi.org/10.1002/batt.202200415.

96. Hallemans, N., Howey, D., Battistel, A., Saniee, N.F., Scarpioni, F., Wouters, B., La Mantia, F., Hubin, A., Widanage, W.D., and Lataire, J. (2023). Electrochemical impedance spectroscopy beyond linearity and stationarity—A critical review. Electrochim. Acta *466*, 142939. https://doi.org/10.1016/j.electacta.2023.142939.

97. Rüther, T., Schamel, M., Plank, C., Schomburg, F., Röder, F., and Danzer, M.A. (2023). Cell-to-Cell-Variations of a Panasonic NCR18650B. zenodo. https://doi.org/10.5281/zenodo.8369275.

98. Tanim, T.R., Dufek, E.J., and Sazhin, S.V. (2021). Challenges and needs for system-level electrochemical lithium-ion battery management and diagnostics. MRS Bull. *46*, 420–428. https://doi.org/10.1557/s43577-021-00101-8.

99. Zhu, L., Wang, J., Wang, Y., Pan, B., and Wang, L. (2024). Detection of Impedance Inhomogeneity in Lithium-Ion Battery Packs Based on Local Outlier Factor. Energies *17*, 5123. https://doi.org/10.3390/en17205123.

100. Raijmakers, L.H.J., Shivakumar, K.M., Donkers, M.C.F., Lammers, M.J.G., and Bergveld, H.J. (2016). Crosstalk Interferences on Impedance Measurements in Battery Packs. IFAC-PapersOnLine *49*, 42–47. https://doi.org/10.1016/j.ifacol.2016.08.007.

101. Beelen, H., Mundaragi Shivakumar, K., Raijmakers, L., Donkers, M.C.F., and Bergveld, H.J. (2020). Towards impedance–based temperature estimation for Li–ion battery packs. Int. J. Energy Res. *44*, 2889–2908. https://doi.org/10.1002/er.5107.

102. Saccoccio, M., Wan, T.H., Chen, C., and Ciucci, F. (2014). Optimal Regularization in Distribution of Relaxation Times applied to Electrochemical Impedance Spectroscopy: Ridge and Lasso Regression Methods - A Theoretical and Experimental Study. Electrochim. Acta *147*, 470–482. https://doi.org/10.1016/j.electacta.2014.09.058.

103. Paul, T., Chi, P.W., Wu, P.M., and Wu, M.K. (2021). Computation of distribution of relaxation times by Tikhonov regularization for Li ion batteries: usage of L-curve method. Sci. Rep. *11*, 12624. https://doi.org/10.1038/s41598-021-91871-3.

104. Maradesa, A., Py, B., Wan, T.H., Effat, M.B., and Ciucci, F. (2023). Selecting the Regularization Parameter in the Distribution of Relaxation Times. J. Electrochem. Soc. *170*, 030502. https://doi.org/10.1149/1945-7111/acbca4.

105. Hahn, M., Schindler, S., Triebs, L.C., and Danzer, M.A. (2019). Optimized Process Parameters for a Reproducible Distribution of Relaxation Times Analysis of Electrochemical Systems. Batteries *5*, 43. https://doi.org/10.3390/batteries5020043.

106. Rüther, T., Hileman, W., Plett, G.L., Trimboli, M.S., and Danzer, M.A. (2024). Demystifying the Distribution of Relaxation Times: A Simulation-Based Investigation into the Limits and Possibilities of Interpretation for Lithium-Ion Batteries. J. Electrochem. Soc. *171*, 060508. https://doi.org/10.1149/1945-7111/ad4fe5.

107. Danzer, M.A. (2019). Generalized Distribution of Relaxation Times Analysis for the Characterization of Impedance Spectra. Batteries *5*, 53. https://doi.org/10.3390/batteries5030053.

108. IVERS-TIFFÉE, E., and Weber, A. (2017). Evaluation of electrochemical impedance spectra by the distribution of relaxation times. J. Ceram. Soc. Japan *125*, 193–201. https://doi.org/10.2109/jcersj2.16267.

109. Plank, C., Rüther, T., Jahn, L., Schamel, M., Schmidt, J.P., Ciucci, F., and Danzer, M.A. (2024). A review on the distribution of relaxation times analysis: A powerful tool for process identification of electrochemical systems. J. Power Sources *594*, 233845. https://doi.org/10.1016/j.jpowsour.2023.233845.

110. Maradesa, A., Py, B., Huang, J., Lu, Y., Iurilli, P., Mrozinski, A., Law, H.M., Wang, Y., Wang, Z., Li, J., et al. (2024). Advancing electrochemical impedance analysis through innovations in the distribution of relaxation times method. Joule *8*, 1958–1981. https://doi.org/10.1016/j.joule.2024.05.008.

111. Lu, Y., Zhao, C.Z., Huang, J.Q., and Zhang, Q. (2022). The timescale identification decoupling complicated kinetic processes in lithium batteries. Joule *6*, 1172–1198. https://doi.org/10.1016/j.joule.2022.05.005.

112. Schmidt, J.P., and Ivers-Tiffée, E. (2016). Pulse-fitting – A novel method for the evaluation of pulse measurements, demonstrated for the low frequency behavior of lithium-ion cells. J. Power Sources *315*, 316–323. https://doi.org/10.1016/j.jpowsour.2016.03.026.

113. Goldammer, E., and Kowal, J. (2021). Determination of the Distribution of Relaxation Times by Means of Pulse Evaluation for Offline and Online Diagnosis of Lithium-Ion Batteries. Batteries *7*, 36. https://doi.org/10.3390/batteries7020036.

114. Wildfeuer, L., Gieler, P., and Karger, A. (2021). Combining the Distribution of Relaxation Times from EIS and Time-Domain Data for Parameterizing Equivalent Circuit Models of Lithium-Ion Batteries. Batteries *7*, 52. https://doi.org/10.3390/batteries7030052.

115. USABC (1996). Electric Vehicle Battery Test Procedures Manual. Revision 2. https://doi.org/10.2172/214312.

116. IEC 62660-1:2018 (2018). Secondary lithium-ion cells for the propulsion of electric road vehicles - Part 1: Performance testing. VDE.

117. ISO 12405-4:2018 (2018). Electrically propelled road vehicles —Test specification for lithium-ion traction battery packs and systems: Part 4: Performance testing.

118. Waag, W., Käbitz, S., and Sauer, D.U. (2013). Experimental investigation of the lithium-ion battery impedance characteristic at various conditions and aging states and its influence on the application. Appl. Energy *102*, 885–897. https://doi.org/10.1016/j.apenergy.2012.09.030.

119. Hentunen, A., Lehmuspelto, T., and Suomela, J. (2014). Time-Domain Parameter Extraction Method for Thévenin-Equivalent Circuit Battery Models. IEEE Trans. Energy Convers. *29*, 558–566. https://doi.org/10.1109/TEC.2014.2318205.

120. Plett, G.L. (2025). A Linear Method to Fit Equivalent Circuit Model Parameter Values to HPPC Relaxation Data From Lithium-Ion Cells. ASME Letters in Dynamic Systems and Control *5*, 4066626. https://doi.org/10.1115/1.4066626.

121. Weppner, W., and Huggins, R.A. (1977). Determination of the Kinetic Parameters of Mixed–Conducting Electrodes and Application to the System Li3Sb. J. Electrochem. Soc. *124*, 1569–1578. https://doi.org/10.1149/1.2133112.

122. Kim, J., Park, S., Hwang, S., and Yoon, W.S. (2022). Principles and Applications of Galvanostatic Intermittent Titration Technique for Lithium-ion Batteries. J. Electrochem. Sci. Technol. *13*, 19–31. https://doi.org/10.33961/jecst.2021.00836.

123. Cabañero, M.A., Boaretto, N., Röder, M., Müller, J., Kallo, J., and Latz, A. (2018). Direct Determination of Diffusion Coefficients in Commercial Li-Ion Batteries. J. Electrochem. Soc. *165*, A847–A855. https://doi.org/10.1149/2.0301805jes.

124. Huber, C., Horsche, M., Brand, M.J., and Schmidt, K. (2019). Method, apparatus and computer program for determining an impedance of an electrically conducting device. European patent EP3438682A1, filed December 20, 2017 and granted June 7, 2023.

125. Brand, M.J. (2018). Lithium-ion battery cells and systems under dynamic electric loads (Herbert Utz Verlag).

126. Zhao, X., Wang, Z., Li, E., and Miao, H. (2024). Investigation into Impedance Measurements for Rapid Capacity Estimation of Lithium-ion Batteries in Electric Vehicles. Journal of Dynamics, Monitoring and Diagnostics *3*, 21. https://doi.org/10.37965/jdmd.2024.475.

127. Bohlen, O. (2008). Impedance-based battery monitoring (Shaker Verlag GmbH).

128. Dullau, M., Scholz, T., Kremzow-Tennie, S., Pautzke, F., and Schmuelling, B. (2023). In-Situ State of Health Analysis and Simulation of Electric Vehicle Battery Packs Using Conventional Charging Infrastructure. In 6th International Conference on Electrical Engineering and Green Energy (CEEGE) (IEEE), pp. 236–245. https://doi.org/10.1109/CEEGE58447.2023.10246474.

129. Wang, L., Cheng, Y., and Zhao, X. (2015). Influence of connecting plate resistance upon LiFePO4 battery performance. Appl. Energy *147*, 353–360. https://doi.org/10.1016/j.apenergy.2015.03.016.

130. Wang, Z., Zhao, X., Fu, L., Zhen, D., Gu, F., and Ball, A.D. (2023). A review on rapid state of health estimation of lithium-ion batteries in electric vehicles. Sustain. Energy Technol. Assessments *60*, 103457. https://doi.org/10.1016/j.seta.2023.103457.

131. Ludwig, S., Zilberman, I., Horsche, M.F., Wohlers, T., and Jossen, A. (2021). Pulse resistance based online temperature estimation for lithium-ion cells. J. Power Sources *490*, 229523. https://doi.org/10.1016/j.jpowsour.2021.229523.

132. Cui, Z., Cui, N., Wang, C., Li, C., and Zhang, C. (2021). A Robust Online Parameter Identification Method for Lithium-Ion Battery Model Under Asynchronous Sampling and Noise Interference. IEEE Trans. Ind. Electron. *68*, 9550–9560. https://doi.org/10.1109/TIE.2020.3028799.

133. Reiter, A., Lehner, S., Bohlen, O., and Sauer, D.U. (2022). Electrical cell-to-cell variations within large-scale battery systems — A novel characterization and modeling approach. J. Energy Storage *57*, 106152. https://doi.org/10.1016/j.est.2022.106152.

134. Moral, C.G., Laborda, D.F., Alonso, L.S., Guerrero, J.M., Fernandez, D., Rivas Pereda, C., and Reigosa, D.D. (2020). Battery Internal Resistance Estimation Using a Battery Balancing System Based on Switched Capacitors. IEEE Trans. Ind. Appl. *56*, 5363–5374. https://doi.org/10.1109/TIA.2020.3005382.

135. Tang, X., Lai, X., Liu, Q., Zheng, Y., Zhou, Y., Ma, Y., and Gao, F. (2023). Predicting battery impedance spectra from 10-second pulse tests under 10 Hz sampling rate. iScience *26*, 106821. https://doi.org/10.1016/j.isci.2023.106821.

136. Dubarry, M., Truchot, C., and Liaw, B.Y. (2012). Synthesize battery degradation modes via a diagnostic and prognostic model. J. Power Sources *219*, 204–216. https://doi.org/10.1016/j.jpowsour.2012.07.016.

137. Birkl, C.R., Roberts, M.R., McTurk, E., Bruce, P.G., and Howey, D.A. (2017). Degradation diagnostics for lithium ion cells. J. Power Sources *341*, 373–386. https://doi.org/10.1016/j.jpowsour.2016.12.011.

138. Balewski, L., and Brenet, J.P. (1967). A New Method for the Study of the Electrochemical Reactivity of Manganese Dioxide. Electrochemical Technology *5*, 527–531.

139. Barker, J., Saidi, M.Y., and Swoyer, J.L. (2003). A Sodium-Ion Cell Based on the Fluorophosphate Compound NaVPO[sub 4]F. Electrochem. Solid State Lett. *6*, A1. https://doi.org/10.1149/1.1523691.

140. Sieg, J., Storch, M., Fath, J., Nuhic, A., Bandlow, J., Spier, B., and Sauer, D.U. (2020). Local degradation and differential voltage analysis of aged lithium-ion pouch cells. J. Energy Storage *30*, 101582. https://doi.org/10.1016/j.est.2020.101582.

141. Bloom, I., Christophersen, J., and Gering, K. (2005). Differential voltage analyses of high-power, lithium-ion cells. 2. Applications. J. Power Sources *139*, 304–313. https://doi.org/10.1016/j.jpowsour.2004.07.022.

142. Dubarry, M., and Anseán, D. (2022). Best practices for incremental capacity analysis. Front. Energy Res. *10*, 1023555. https://doi.org/10.3389/fenrg.2022.1023555.

143. Barai, A., Uddin, K., Dubarry, M., Somerville, L., McGordon, A., Jennings, P., and Bloom, I. (2019). A comparison of methodologies for the non-invasive characterisation of commercial Li-ion cells. Prog. Energy Combust. Sci. *72*, 1–31. https://doi.org/10.1016/j.pecs.2019.01.001.

144. Dubarry, M., Vuillaume, N., and Liaw, B.Y. (2009). From single cell model to battery pack simulation for Li-ion batteries. J. Power Sources *186*, 500–507. https://doi.org/10.1016/j.jpowsour.2008.10.051.

145. Kim, J., and Cho, B.H. (2012). Stable Configuration of a Li-Ion Series Battery Pack Based on a Screening Process for Improved Voltage/SOC Balancing. IEEE Trans. Power Electron. *17*, 411–424.

146. Jiang, Y., Jiang, J., Zhang, C., Zhang, W., Gao, Y., and Guo, Q. (2017). Recognition of battery aging variations for LiFePO 4 batteries in 2nd use applications combining incremental capacity analysis and statistical approaches. J. Power Sources *360*, 180–188. https://doi.org/10.1016/j.jpowsour.2017.06.007.

147. Xu, Z., Wang, J., Lund, P.D., and Zhang, Y. (2021). Estimation and prediction of state of health of electric vehicle batteries using discrete incremental capacity analysis based on real driving data. Energy *225*, 120160. https://doi.org/10.1016/j.energy.2021.120160.

148. Chang, L., Wang, C., Zhang, C., Xiao, L., Cui, N., Li, H., and Qiu, J. (2020). A novel fast capacity estimation method based on current curves of parallel-connected cells for retired lithium-ion batteries in second-use applications. J. Power Sources *459*, 227901. https://doi.org/10.1016/j.jpowsour.2020.227901.

149. Krupp, A., Ferg, E., Schuldt, F., Derendorf, K., and Agert, C. (2020). Incremental Capacity Analysis as a State of Health Estimation Method for Lithium-Ion Battery Modules with Series-Connected Cells. Batteries *7*, 7010002. https://doi.org/10.3390/batteries7010002.

150. Jiang, T., Sun, J., Wang, T., Tang, Y., Chen, S., Qiu, S., Liu, X., Lu, S., and Wu, X. (2021). Sorting and grouping optimization method for second-use batteries considering aging mechanism. J. Energy Storage *44*, 103264. https://doi.org/10.1016/j.est.2021.103264.

151. Singh, A., Lodge, A., Li, Y., Widanage, W.D., and Barai, A. (2023). A new method to perform Lithium-ion battery pack fault diagnostics – Part 1: Algorithm development and its performance analysis. Energy Rep. *10*, 4474–4490. https://doi.org/10.1016/j.egyr.2023.11.008.

152. Dubarry, M., Tun, M., Baure, G., Matsuura, M., and Rocheleau, R.E. (2021). Battery Durability and Reliability under Electric Utility Grid Operations: Analysis of On-Site Reference Tests. Electronics *10*, 10131593. https://doi.org/10.3390/electronics10131593.

153. Dubarry, M., and Beck, D. (2024). Investigation of the impact of different electrode inhomogeneities on the voltage response of Li-ion batteries. Cell Reports Physical Science *5*, 102138. https://doi.org/10.1016/j.xcrp.2024.102138.

154. Bandla, V.N., Briot, L., Bernard, J., Petit, M., Morcrette, M., and Delacourt, C. (2024). Modeling the internal inhomogeneous aging behavior within individual Li-ion cells – During cycle aging. J. Energy Storage *86*, 111186. https://doi.org/10.1016/j.est.2024.111186.

155. Dubarry, M., Truchot, C., Devie, A., and Liaw, B.Y. (2015). State-of-Charge Determination in Lithium-Ion Battery Packs Based on Two-Point Measurements in Life. J. Electrochem. Soc. *162*, A877–A884. https://doi.org/10.1149/2.0201506jes.

156. Feng, X., Xu, C., He, X., Wang, L., Gao, S., and Ouyang, M. (2019). A graphical model for evaluating the status of series-connected lithium-ion battery pack. Int. J. Energy Res. *43*, 749–766. https://doi.org/10.1002/er.4305.

157. Lu, Y., Chen, X., Han, X., Guo, D., Wang, Y., Feng, X., and Ouyang, M. (2024). Mechanisms for the evolution of cell-to-cell variations and their impacts on fast-charging performance within a lithium-ion battery pack. J. Energy Chem. *99*, 11–22. https://doi.org/10.1016/j.jechem.2024.07.026.

158. Naguib, M., Kollmeyer, P., and Emadi, A. (2021). Lithium-Ion Battery Pack Robust State of Charge Estimation, Cell Inconsistency, and Balancing: Review. IEEE Access *9*, 50570–50582. https://doi.org/10.1109/access.2021.3068776.

159. Wind, J., and Vie, P.J.S. (2024). Revisiting Pulse-Based OCV Incremental Capacity Analysis for Diagnostics of Li-Ion Batteries. Batteries *10*, 10080277. https://doi.org/10.3390/batteries10080277.

160. Dubarry, M., and Beck, D. (2022). Perspective on Mechanistic Modeling of Li-Ion Batteries. Acc. Mater. Res. *3*, 843–853. https://doi.org/10.1021/accountsmr.2c00082.

161. Dubarry, M., Costa, N., and Matthews, D. (2023). Data-driven direct diagnosis of Li-ion batteries connected to photovoltaics. Nat. Commun. *14*, 3138. https://doi.org/10.1038/s41467-023-38895-7.

162. Dubarry, M., and Beck, D. (2020). Big data training data for artificial intelligence-based Li-ion diagnosis and prognosis. J. Power Sources *479*, 228806. https://doi.org/10.1016/j.jpowsour.2020.228806.

163. Dubarry, M., Berecibar, M., Devie, A., Anseán, D., Omar, N., and Villarreal, I. (2017). State of health battery estimator enabling degradation diagnosis: Model and algorithm description. J. Power Sources *360*, 59–69. https://doi.org/10.1016/j.jpowsour.2017.05.121.

164. Hofmann, T., Hamar, J., Mager, B., Erhard, S., and Schmidt, J.P. (2024). Transfer learning from synthetic data for open-circuit voltage curve reconstruction and state of health estimation of lithium-ion batteries from partial charging segments. Energy and AI *17*, 100382. https://doi.org/10.1016/j.egyai.2024.100382.

165. Hua, Y., Zhou, S., Cui, H., Liu, X., Zhang, C., Xu, X., Ling, H., and Yang, S. (2020). A comprehensive review on inconsistency and equalization technology of lithium–ion battery for electric vehicles. International Journal of Energy Research. https://doi.org/10.1002/er.5683.

166. Neupert, S., and Kowal, J. (2018). Inhomogeneities in Battery Packs. World Electric Vehicle Journal *9*, 9020020. https://doi.org/10.3390/wevj9020020.

167. Chang, L., Ma, C., Zhang, C., Duan, B., Cui, N., and Li, C. (2023). Correlations of lithium-ion battery parameter variations and connected configurations on pack statistics. Appl. Energy *329*, 120275. https://doi.org/10.1016/j.apenergy.2022.120275.

168. Feng, F., Hu, X., Hu, L., Hu, F., Li, Y., and Zhang, L. (2019). Propagation mechanisms and diagnosis of parameter inconsistency within Li-Ion battery packs. Renew. Sustain. Energy Rev. *112*, 102–113. https://doi.org/10.1016/j.rser.2019.05.042.

169. Baumann, M., Wildfeuer, L., Rohr, S., and Lienkamp, M. (2018). Parameter variations within Li-Ion battery packs – Theoretical investigations and experimental quantification. J. Energy Storage *18*, 295–307. https://doi.org/10.1016/j.est.2018.04.031.